THE JOURNAL OF BIOLOGICAL CHEMISTRY VOL. 283, NO. 10, pp. 6476–6488, March 7, 2008

Caveolin Regulates Endocytosis of the Muscle Repair Protein, Dysferlin*[S]

Received for publication, October 24, 2007, and in revised form, November 26, 2007 Published, JBC Papers in Press, December 20, 2007, DOI 10.1074/jbc.M708776200

Delia J. Hernández-Deviez[‡], Mark T. Howes[‡], Steven H. Laval[§], Kate Bushby[§], John F. Hancock[‡], and Robert G. Parton[‡¶1]

From the [‡]Institute for Molecular Bioscience, [¶]Centre for Microscopy and Microanalysis, University of Queensland, Brisbane, Queensland 4072, Australia and the [§]Institute of Human Genetics, International, Centre for Life, Newcastle NE1 3BZ, United Kingdom

Dysferlin and Caveolin-3 are plasma membrane proteins associated with muscular dystrophy. Patients with mutations in the *CAV3* gene show dysferlin mislocalization in muscle cells. By utilizing caveolin-null cells, expression of caveolin mutants, and different mutants of dysferlin, we have dissected the site of action of caveolin with respect to dysferlin trafficking pathways. We now show that Caveolin-1 or -3 can facilitate exit of a dysferlin mutant that accumulates in the Golgi complex of *Cav1*$^{-/-}$ cells. In contrast, wild type dysferlin reaches the plasma membrane but is rapidly endocytosed in *Cav1*$^{-/-}$ cells. We demonstrate that the primary effect of caveolin is to cause surface retention of dysferlin. Caveolin-1 or Caveolin-3, but not specific caveolin mutants, inhibit endocytosis of dysferlin through a clathrin-independent pathway colocalizing with internalized glycosylphosphatidylinositol-anchored proteins. Our results provide new insights into the role of this endocytic pathway in surface remodeling of specific surface components. In addition, they highlight a novel mechanism of action of caveolins relevant to the pathogenic mechanisms underlying caveolin-associated disease.

Dysferlin and Caveolin-3 (muscle-specific caveolin, Cav3) are sarcolemmal proteins whose role in muscle has gained clinical attention because mutations in their genes are associated with a number of muscle pathologies. Patients with mutations in the *dysferlin* (*DYSF*) gene develop disorders such as limb girdle muscular dystrophy type 2B, miyoshi myopathy, and distal myopathy (1–5). Whereas disruption in the Caveolin-3 (*CAV3*) gene has been linked to limb girdle muscular dystrophy 1C, Rippling muscle diseases, hyperCKemia, and distal myopathy among other myopathies (6–15). Dysferlin and Cav3 have been co-purified from muscle cells (16, 17) and shown to localize to adjacent membrane domains at the surface in mature muscle fibers (18). Moreover, dysferlin is depleted from the plasma membrane (PM)[2] when Cav3 is mutated (8, 9, 14, 17, 19). We have recently demonstrated a role for caveolin in dysferlin localization at the PM (18). However, the interplay of dysferlin and caveolin membrane trafficking dynamics remains to be examined.

Dysferlin belongs to the ferlin family of proteins comprising otoferlin, myoferlin, and fer1L3 (20–22). The *DYSF* gene encodes a 230-kDa skeletal muscle membrane protein (2, 5, 23) with homology to the *Caenorhabditis elegans* sperm-vesicle fusion factor, *fer-1* (2). Because of this dysferlin has been suggested to play a role in vesicle fusion in skeletal muscle (2, 24). Moreover, in the absence of dysferlin muscle cells show defective resealing of membrane disruptions (25). Dysferlin has a single transmembrane domain at the C terminus and a long N-terminal cytoplasmic region containing six C2 domains. C2 domains are a common feature of the synaptotagmin family of proteins implicated in vesicular traffic and membrane fusion events through calcium-dependent interactions with phospholipids and proteins (26–29). Interestingly, dysferlin and synaptotagmins share structural similarities (20, 24) further implicating dysferlin in membrane trafficking processes.

In mammalian cells, the *CAV* gene family consists of three isoforms: Caveolin-1, -2, and -3 (30–35), which are crucial structural components of caveolar membranes (~65 nm, uncoated flask-shaped PM pits). Caveolins are 21–24-kDa integral membrane proteins, Caveolin-1 (Cav1) and -2 (Cav2) are mainly co-expressed in non-muscle cells, whereas Cav3 is largely expressed in skeletal and cardiac muscle but is also found in some smooth muscle (36, 37). Caveolins are cholesterol- and fatty acid-binding proteins, and are thought to play a role in vesicular traffic and signal transduction events (38–42). The protein structure of caveolins is characterized by a hairpin loop topology with a hydrophobic region immersed in the lipid bilayer (the intramembrane domain), and both N and C terminus regions facing the cytoplasm (43–45). Additionally, the conserved juxtamembrane region, the caveolin scaffolding

* This work was supported by grants from the National Health and Medical Research Council of Australia (to R. G. P. and J. F. H.), the Muscular Dystrophy Campaign, Association Francais contre les Myopathies, and the Jain Foundation (to K. B. and S. H. L.). The costs of publication of this article were defrayed in part by the payment of page charges. This article must therefore be hereby marked "*advertisement*" in accordance with 18 U.S.C. Section 1734 solely to indicate this fact.

[S] The on-line version of this article (available at http://www.jbc.org) contains supplemental Figs. S1 and S2.

[1] To whom correspondence should be addressed: Institute for Molecular Bioscience, University of Queensland, Brisbane QLD 4072, Australia. Tel.: 61-7-3346-2032; Fax: 61-7-3346-2339; E-mail: R.Parton@imb.uq.edu.au.

[2] The abbreviations used are: PM, plasma membrane; Cav, Caveolin; Cav1$^{-/-}$, Cav1$^{-/-}$ immortalized cell lines; CSD, caveolin scaffolding domain; CTB, cholera toxin binding subunit; GPI-AP, glycosylphosphatidylinositol-anchored proteins; GEECs, GPI-AP-enriched early endosomal compartments; Tfn, transferrin; WT, wild type; AA, ascorbic acid; HA, hemagglutinin; GFP, green fluorescent protein; HRP, horseradish peroxidase; MEF, mouse embryonic fibroblasts; DAB, dimethylaminoazobenzene; IC, intracellular; TM, transmembrane.

domain (CSD), has been shown to bind *in vitro* to a consensus sequence ($\phi X\phi XXXX\phi XX\phi$, ϕ aromatic residues, X any amino acid) (46) present in various proteins. Dysferlin has several putative CSD binding motifs (17).

We have recently described the subcellular distribution of dysferlin with respect to Cav3 and showed that dysferlin association with the PM is impaired in the absence of caveolin, or in the presence of dystrophy-associated mutant forms of Cav3 (18). Although Cav3 and dysferlin copurify (16, 17), the precise interacting domains and roles in their trafficking dynamics are poorly understood. We show here that in the absence of caveolin, dysferlin reaches the PM but is rapidly endocytosed through a caveolin-, clathrin-, and dynamin-independent pathway. Wild type caveolin, but not mutant forms of caveolin associated with muscle disease, specifically inhibit dysferlin endocytosis causing its retention at the cell surface.

EXPERIMENTAL PROCEDURES

DNA Constructs, Reagents, and Antibodies—Cell culture reagents were obtained from Invitrogen. The antibodies used were: mouse anti-LBPA, mouse anti-LAMP-1 (Southern Biotech), mouse anti-GM130 (BD Biosciences), rabbit antibody made against the conserved region of Cav3 (47), rabbit anti-HA (Dr. T. Nilsson, Gothenburg University, Gothenburg, Sweden), rabbit anti-GFP (48), mouse anti-myc 9B11 (Cell Signaling Technology), and anti-protein-disulfide isomerase. Secondary antibodies conjugated to Alexa Fluor 488, 350, 546, 647, and CTB conjugated to Alexa Fluor 555 and Tf-Alexa Fluor 647 (Molecular Probes), CY3-conjugated anti-mouse antibody (Jackson Immunoresearch), and HRP-conjugated secondary antibodies (Zymed Laboratories) were used. SuperSignal substrate was obtained from Pierce Chemical Company. All other chemicals and reagents were obtained from Sigma.

GFP-dysferlin cDNA was used as a template to generate different truncation mutants by restriction digestion at unique enzymatic sites (49) (see Fig. 1), GFPΔ-C2 (GFP-TM), GFPΔ-1 (GFP3′GFP-2), GFPΔ-2 (GFP-Tth), GFPΔ-3 (GFP-Xho), and GFP-Δ-TM. Expression of the complete fusion proteins was confirmed in multiple cell lines. Cav3G55S-HA, Cav3C71W-HA, and Flotillin-HA were made as described (50, 51). The glycosylphosphatidylinositol (GPI)-GFP, Cav1Δ81–100-HA, and transferrin receptor constructs were gifts from C. Zurzolo (Institut Pasteur, France), D. Brown (State University of New York), S. L. Schmid (Scripps Research Institute), and V. Gerke (Center for Molecular Biology of Inflammation, ZMBE), respectively. Dynamin inhibitor, dynasore, was a kind gift from T. Kirchhausen (Harvard Medical School).

Cell Culture and Transfection—We utilized immortalized mouse embryonic fibroblasts (MEF) cell lines derived from *Cav1* WT or knock-out mice as in previous studies (18, 52, 53). Cells were grown on glass coverslips and cDNAs were transiently expressed utilizing Lipofectamine 2000 (Invitrogen) according to the manufacturer's directions.

Immunofluorescence and Microscopy—Immunolabeling of MEFs were carried out as described previously (18). Confocal images were acquired with an inverted Zeiss LSM 510 META microscope system (Axiovert 200M, Carl Zeiss MicroImaging) under a Plan apochromatic ×63 1.4 NA oil immersion objective. Images were processed and merged using Adobe Photoshop 9.0 software. Identical imaging and processing parameters were used for all figures.

Surface Labeling and Single Cell Fluorescence Quantification—Surface labeling and quantification of the fluorescence intensity of dysferlin pool at the PM was performed as described previously (18). The average pixel intensity for PM and IC/Golgi pools were measured using Adobe Photoshop 9.0 software. Experiments were repeated three times.

Quantifications shown in Figs. 1*D*, 2*C*, 3*B*, and 7*B* are representative of 3 individual experiments and were performed once on 250–350 cells and twice on a total of 30 cells for each construct. Subcellular phenotypes were determined based on colabeling with relevant IC markers. Results are presented as percentage of cells showing a common phenotype.

Myc, Tfn, CTB, and GPI Uptake Assays—Uptake assays were performed as described previously (54). In brief, 20 mg/ml monoclonal anti-myc antibody, 1 mg/ml CTxB-Alexa Fluor 555, or 5 mg/ml Tfn Alexa Fluor 647 was bound to cells on ice for 30 min in CO_2-independent medium. Cells were washed with ice-cold CO_2-independent medium to remove unbound reagent prior to uptake in growth media (10% fetal bovine serum, 2 mM L-glutamine/Dulbecco's modified Eagle's medium) at 37 °C, for the times indicated. Cells were placed on ice-cold CO_2-independent medium and washed 2 times for 30 s in 0.5 M glycine (pH 2.2). The cells were fixed in 2% paraformaldehyde and processed for immunofluorescence. For inhibition of dynamin-dependent uptake, cells were preincubated in either 80 mM dynasore/growth media or 0.4% Me_2SO/growth media for 30 min at 37 °C, followed by Tfn and anti-myc uptake in the presence or absence of dynasore.

Ultrastructural Analysis of Dysferlin Endocytosis in WT Cav1 and Cav1$^{-/-}$ MEFs—WT *Cav1* or *Cav1*$^{-/-}$ MEFs were transfected with GFPDysf. After overnight incubation, to allow expression of the constructs, the cells were incubated with mouse anti-myc antibodies at 4 °C for 20 min, washed, and further incubated with anti-mouse HRP at 4 °C for 20 min. The cells were warmed to 37 °C for 2 min to allow uptake and then incubated in DAB, with or without ascorbic acid (AA), fixed, and processed for resin embedding, exactly as described previously (54). Due to the low transfection efficiency, GFP-expressing cells were identified by light microscopy before processing. They were marked to allow subsequent location for sectioning. Quantitation of PM coverage of the HRP reaction product was by intersection counting. The number of intersections of a square lattice grid with unlabeled and DAB-covered areas of the PM in random areas of transfected WT *Cav1* or *Cav1*$^{-/-}$ MEFs was measured on digital images to gain an estimate of PM coverage by the HRP reaction.

RESULTS

Subcellular Distribution of Dysferlin Truncation Mutants in WT Cav1 and Cav1$^{-/-}$ MEF Cells—To better understand the functional link between dysferlin and Cav3 we examined the subcellular distribution of truncation mutants of dysferlin and analyzed their trafficking dependence on caveolin. We used WT *Cav1* and *Cav1*$^{-/-}$ MEFs as a model system. *Cav1*$^{-/-}$ cells have no detectable caveolae as they lack Cav1 (as well as the

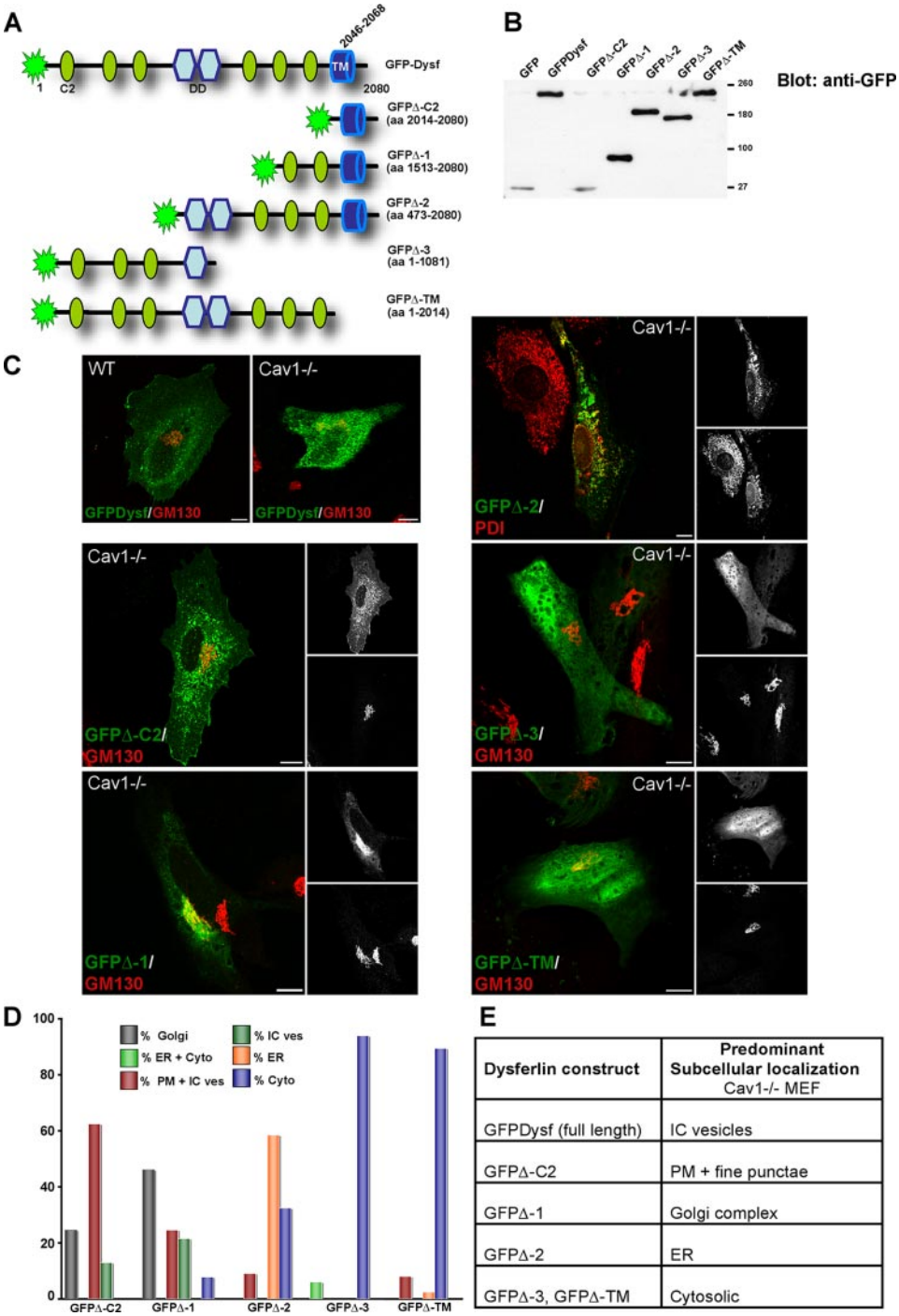

Dysferlin construct	Predominant Subcellular localization Cav1-/- MEF
GFPDysf (full length)	IC vesicles
GFPΔ-C2	PM + fine punctae
GFPΔ-1	Golgi complex
GFPΔ-2	ER
GFPΔ-3, GFPΔ-TM	Cytosolic

FIGURE 1. **Subcellular distribution of dysferlin truncation mutants in *Cav1*$^{-/-}$ cells.** *A*, schematic representations of full-length and truncation mutants of GFPDysf. *B*, baby hamster kidney cells were transfected with either GFP or different GFPDysf constructs. Total cell lysates were separated in a 5.5% SDS gel, electrotransferred, and immunoblotted using anti-GFP antibody. Truncated GFP-tagged mutants appear as single polypeptides of predicted sizes. *C*, full-length dysferlin, GFPDysf, is mainly targeted to the PM or to intracellular vesicles in WT *Cav1* or *Cav1*$^{-/-}$ MEFs, respectively. GFPΔ-C2 is mainly targeted to the PM and to fine punctate structures. GFPΔ-1 predominantly accumulates in the Golgi as demonstrated by colocalization with the Golgi marker, GM130. GFPΔ-2 is mostly concentrated in endoplasmic reticulum shown by the extensive overlay with protein-disulfide isomerase, an endoplasmic reticulum marker, whereas GFPΔ-3 and GFPΔ-TM are predominantly cytosolic. *D*, predominant subcellular phenotypes were scored based on colabeling with relevant intracellular markers. Results are presented as percentage of cells showing a prevalent phenotype, and are representative of three individual experiments (n = 30–350/for each construct). *E*, summary table of dysferlin constructs and subcellular localizations. *Bar*, 10 μm.

muscle-specific isoform Cav3). This represents a powerful model system to analyze dysferlin trafficking with respect to caveolin re-expression rescues the dysferlin trafficking defects (18).

Truncated versions of dysferlin with an N-terminal GFP tag were generated (see summary in Fig. 1). Expression of these mutants in baby hamster kidney cells showed single bands of the predicted molecular weight for each of the truncation mutants (Fig. 1*B*). We compared the subcellular distribution of the mutant proteins to the WT protein by heterologous expression of truncation mutant forms of dysferlin in WT *Cav1* or *Cav1*$^{-/-}$ MEFs (refer to summary table in Fig. 1). Full-length dysferlin efficiently reaches the PM in WT *Cav1* MEFs (Fig. 1*C*), consistent with previous results (18). In contrast, dysferlin localized to intracellular structures but not to the Golgi complex in *Cav1*$^{-/-}$ cells (Fig. 1*C*). GFPΔ-2, which lacks the three first C2 domains, was found to mainly localize to the endoplasmic reticulum as judged by a large overlap with the endoplasmic reticulum marker, protein-disulfide isomerase (Fig. 1, *C–E*). Truncated versions of dysferlin lacking the TM domain, GFPΔ-3 and GFPΔ-TM, were however, mainly cytosolic (Fig. 1, *C–E*) and were indistinguishable in WT *Cav1* and *Cav1*$^{-/-}$ cells.

In contrast to WT dysferlin and to the above mutants, GFPΔ-1, which lacks the first four C2 domains, mostly accumulated in the Golgi complex of *Cav1*$^{-/-}$ MEFs, as demonstrated by colocalization with the Golgi marker, GM130 (Fig. 1, *C–E*), but associated with the PM in WT *Cav1* MEFs (Figs. 1*C* and 2). To examine whether this reflected a direct role of caveolin in facilitating the transport of GFPΔ-1 to the PM, we co-expressed GFPΔ-1 and HA-tagged Cav1 (Cav1-HA) or Cav3 (Cav3-HA) in *Cav1*$^{-/-}$ MEFs. GFPΔ-1 efficiently exited the Golgi apparatus and reached the PM (Fig. 2). Quantitation showed that in ~66% of *Cav1*$^{-/-}$ MEFs expressing

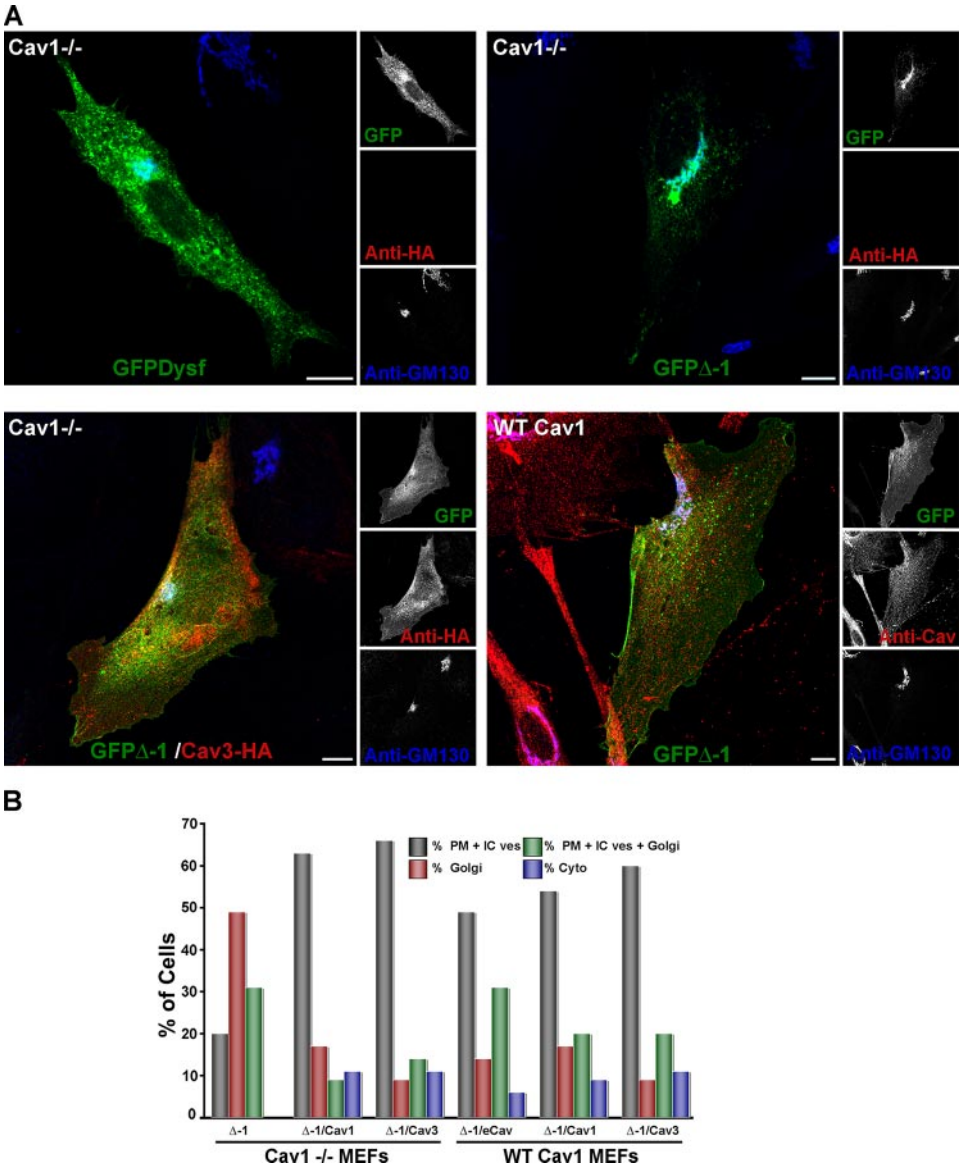

FIGURE 2. **Cav1 and Cav3 redistribute GFPΔ-1 from the Golgi to the plasma membrane in *Cav1*$^{-/-}$ cells.** MEF cells were transfected with GFPDysf or GFPΔ-1 or co-transfected with GFPΔ-1 and epitope-tagged Cav3-HA, and colabeled with anti-HA or anti-Cav and anti-GM130 antibodies. *A*, in *Cav1*$^{-/-}$ cells dysferlin is mainly localized to punctate structures throughout the cytoplasm, whereas GFPΔ-1 mutant accumulates in the Golgi complex as demonstrated by colocalization with the Golgi marker, GM130. Interestingly, expression of epitope-tagged Cav3 redistributes GFPΔ-1 to the PM. Similarly in WT Cav1 MEFs endogenous caveolin is sufficient for GFPΔ-1 Golgi exit and PM targeting. *B*, phenotype quantification. *Cav1*$^{-/-}$ or WT *Cav1* cells expressing GFPΔ-1 or co-expressing GFPΔ-1 and Cav1-HA or Cav3-HA were subject to phenotype scoring. Predominant subcellular phenotypes were scored based on colabeling with relevant intracellular markers. Results are presented as percentage of cells showing a prevalent phenotype, and are representative of three individual experiments (n = 30–350/for each construct). *Bar*, 10 μm.

Cav1-HA or Cav3-HA, GFPΔ-1 was localized to the PM and to intracellular puncta (Fig. 2*B*). GFPΔ-C2, a mutant lacking all six C2 domains was predominantly targeted to the PM in both WT *Cav1* (not shown) and *Cav1*$^{-/-}$ MEFs (Figs. 1, *C–E*, and 3, *A* and *B*). Quantitation of *Cav1*$^{-/-}$ MEFs expressing GFPΔ-C2 showed that in ~97% of the cells, GFPΔ-C2 localized to the PM.

Taken together these results show that GFPΔ-1, which lacks the first four C2 domains, predominantly accumulates in the Golgi complex in the absence of caveolin. This suggests that caveolin is required for GFPΔ-1 transport from the Golgi complex to the PM. In contrast, a mutant lacking all six C2 domains is not retained in the Golgi complex in the presence or absence of caveolin. The loss of all six C2 domains renders mutated dysferlin independent of caveolin for surface delivery.

The fact that GFPΔ-C2 efficiently reached the PM in *Cav1*$^{-/-}$ MEFs (Fig. 3) showed that this truncated protein was not dependent on caveolin for surface targeting. We investigated whether a Golgi-localized dystrophy mutant of Cav3 (Cav3P104L-HA), which causes retention of full-length dysferlin in the Golgi complex (18) would affect the traffic of GFPΔ-C2 to the PM. Cells co-expressing epitope-tagged Cav3P104L (Cav3P104L-HA) and GFPΔ-C2 showed a dramatic accumulation in the Golgi complex (66% of the cells) compared with cells expressing mutated dysferlin alone (4% of the cells) (Fig. 3). Thus GFPΔ-C2, which does not require caveolin for Golgi exit and PM targeting, is blocked in trafficking from the Golgi by the P104L caveolin mutant.

Characterization of Dysferlin Trafficking in Cells Lacking Caveolin—In the absence of caveolin dysferlin accumulates in an intracellular compartment of unknown nature. The identification of these structures should provide insights into the role of caveolins in dysferlin trafficking. We first examined whether dysferlin was targeted for degradation in *Cav1*$^{-/-}$ cells. However, dysferlin failed to co-localize significantly with markers of the late endocytic pathway such as LBPA and LAMP1 (supplemental Fig. S1A). Despite the low surface labeling in the *Cav1*$^{-/-}$ MEFs, we speculated that dysferlin is able to reach the PM but then is efficiently endocytosed in the absence of caveolin. If this was the case, antibodies to the lumenal myc epitope should be readily internalized by *Cav1*$^{-/-}$ cells expressing GFPDysf but not by WT *Cav1* cells. WT *Cav1* and *Cav1*$^{-/-}$ MEFs were transfected with a dysferlin cDNA containing an N-terminal GFP tag and a C-terminal (lumenal/extracellular) myc tag (GFPDysf). After 4 h post-transfection, antibodies against the dysferlin ectoplasmic myc tag were added to the culture medium and antibodies were allowed to internalize overnight. The cells were then fixed, permeabilized, and labeled with secondary antibodies. A striking accumulation

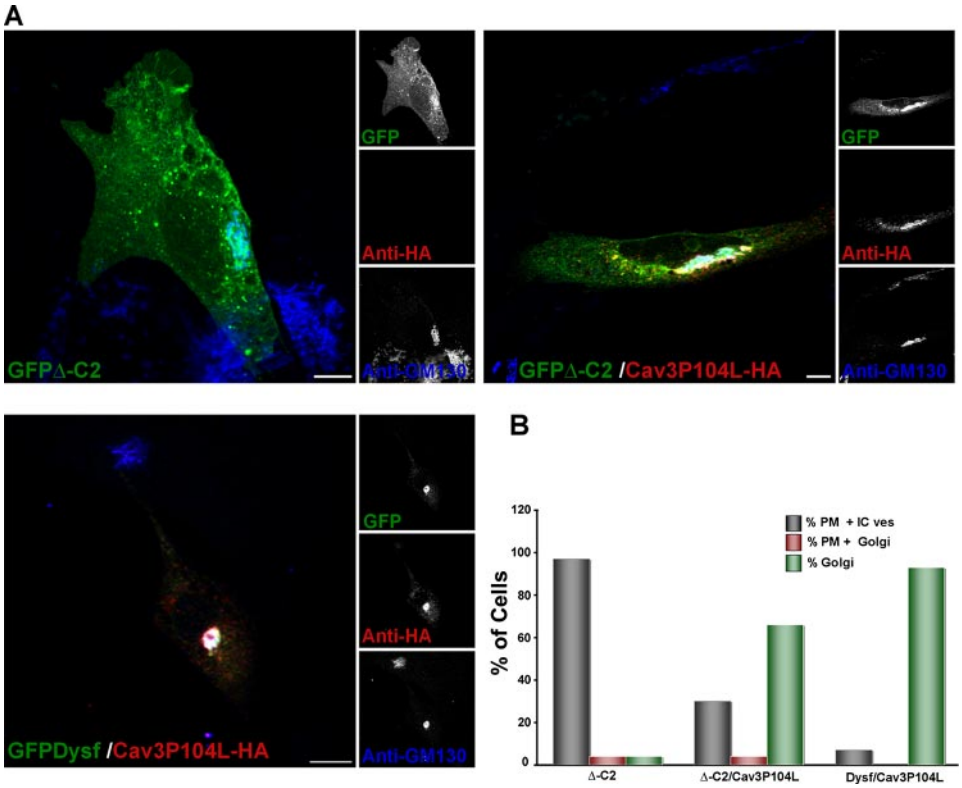

FIGURE 3. **Dystrophy-associated mutant of Cav3 retains GFPΔ-C2 in the Golgi complex.** *Cav1*$^{-/-}$ cells were transfected with GFPΔ-C2 or co-transfected with GFPΔ-C2 or GFPDysf and HA-tagged Cav3P104L, and colabeled with anti-HA and anti-GM130 antibodies. *A*, GFPΔ-C2 is targeted to the PM and punctate structures throughout the cytoplasm. As seen with full-length dysferlin (18), expression of epitope-tagged Cav3P104L-HA causes a dramatic redistribution of GFPΔ-C2 to the Golgi complex as judged by triple labeling with anti-GM130 antibody. *B*, phenotype quantification. *Cav1*$^{-/-}$ cells expressing GFPΔ-C2 or co-expressing GFPΔ-C2 and Cav3P104L-HA or GFPDysf and Cav3P104L-HA were subject to phenotype scoring. Predominant subcellular phenotypes were scored based on colabeling with relevant intracellular markers. Results are presented as percentage of cells showing a prevalent phenotype and are representative of three individual experiments (n = 30–350/for each construct). *Bar*, 10 μm.

of myc antibodies was observed in the *Cav1*$^{-/-}$ MEFs (Fig. 4*A*), very little was internalized in WT *Cav1* and no uptake was observed in neighboring non-transfected cells (see Fig. 4*A*) indicating that the antibodies were taken up specifically after binding to the exposed lumenal myc epitope and not by fluid phase uptake. Consistent with this, the internalized antibodies colocalized with GFPDysf. Identical results were obtained when experiments were performed using Fab fragments against the myc epitope (supplemental Fig. S1B). *Cav1*$^{-/-}$ MEFs expressing GFP-dysf showed higher uptake of Fab fragments compared with WT Cav1 cells (supplemental Fig. S1B). There was no colocalization of Fab fragments and transferrin in WT *Cav1* or *Cav1*$^{-/-}$ cells at any of the time points examined (data not shown).

To investigate this in more detail, myc antibodies were bound to the surface of GFPDysf expressing *Cav1*$^{-/-}$ or WT *Cav1* cells at 4 °C and warmed for 30 min at 37 °C to allow internalization of the antibodies. Surface antibodies were removed by an acid wash. Interestingly, in WT *Cav1* or *Cav1*$^{-/-}$ MEFs, significant GFPDysf internalization was observed after 30 min. Despite the low level of PM dysferlin, *Cav1*$^{-/-}$ MEFs contained many more vesicles positive for both GFP and myc (Fig. 4*B*) suggesting a much higher endocytic rate. This was confirmed by quantitation of the intracellular/PM (IC/PM) ratio after uptake at 10 min (WT *Cav1*, IC/PM ratio = 0.05 ± 0.001; *Cav1*$^{-/-}$, IC/PM ratio = 0.52 ± 0.04) and 40 min (WT *Cav1*, IC/PM ratio = 0.10 ± 0.009; *Cav1*$^{-/-}$, IC/PM ratio = 1.07 ± 0.12) (Fig. 4*C*). Furthermore, and consistent with our previous work (18), we predicted that re-expression of Cav1-HA in *Cav1*$^{-/-}$ MEFs would inhibit dysferlin internalization (Fig. 4*D*). *Cav1*$^{-/-}$ MEFs co-expressing GFPDysf and Cav1-HA showed a distribution of dysferlin similar to that seen in WT *Cav1* MEFs (refer to supplemental Fig. S2A); the ability of dysferlin to reside at the PM membrane has been rescued by expression of Cav-1 (Fig. 4*D* and supplemental Fig. S2A). This was further confirmed by quantifying the amount of internalized myc antibodies in WT *Cav1* and *Cav1*$^{-/-}$ MEFs expressing GFPDysf (WT *Cav1*, 9.06 ± 0.67; *Cav1*$^{-/-}$, 24.04 ± 1.89) or *Cav1*$^{-/-}$ cells co-expressing GFP-dysf and Cav1-HA (9.33 ± 0.56) (refer to "Experimental Procedures") (Fig. 4*D*). Thus these results demonstrate that the major effect of caveolin is to retain dysferlin at the PM and inhibit its internalization. These results demonstrate that dysferlin is not absolutely dependent on caveolin to reach the PM but is efficiently retained at the PM in the presence of caveolin. Taken together, these results show a hitherto unexpected dynamic cycling of dysferlin in *Cav1*$^{-/-}$ cells.

Dysferlin Is Internalized Through a Clathrin-independent Endocytic Pathway—We next examined the pathway by which dysferlin is internalized in *Cav1*$^{-/-}$ MEFs using transferrin to label the clathrin pathway and cholera toxin binding subunit (CTB) or GPI-anchored proteins (AP) as markers of other pathways. Myc antibodies taken up by expressed GFP-dysferlin for various times did not colocalize significantly with transferrin (Fig. 5*A*). However, significant colocalization of internalized myc antibodies and CTB was evident after 2, 10, and 40 min of internalization (Fig. 5*A*). No significant difference in the internalization rate of transferrin or CTB was seen between WT *Cav1* or *Cav1*$^{-/-}$ MEFs (supplemental Fig. S2B).

GPI-AP are internalized via a clathrin- and dynamin-independent endocytic pathway (54–56). To test if dysferlin was trafficking from the PM via this pathway we co-internalized antibodies against the extracellular tags (mouse anti-myc for dysferlin and rabbit anti-GFP for GPI-GFP). *Cav1*$^{-/-}$ MEFs co-expressing GFPDysf and GPI-GFP were labeled on ice with anti-myc and anti-GFP antibodies, warmed to 37 °C for 2, 10, and 40 min, and then acid-washed. Internalized antibodies

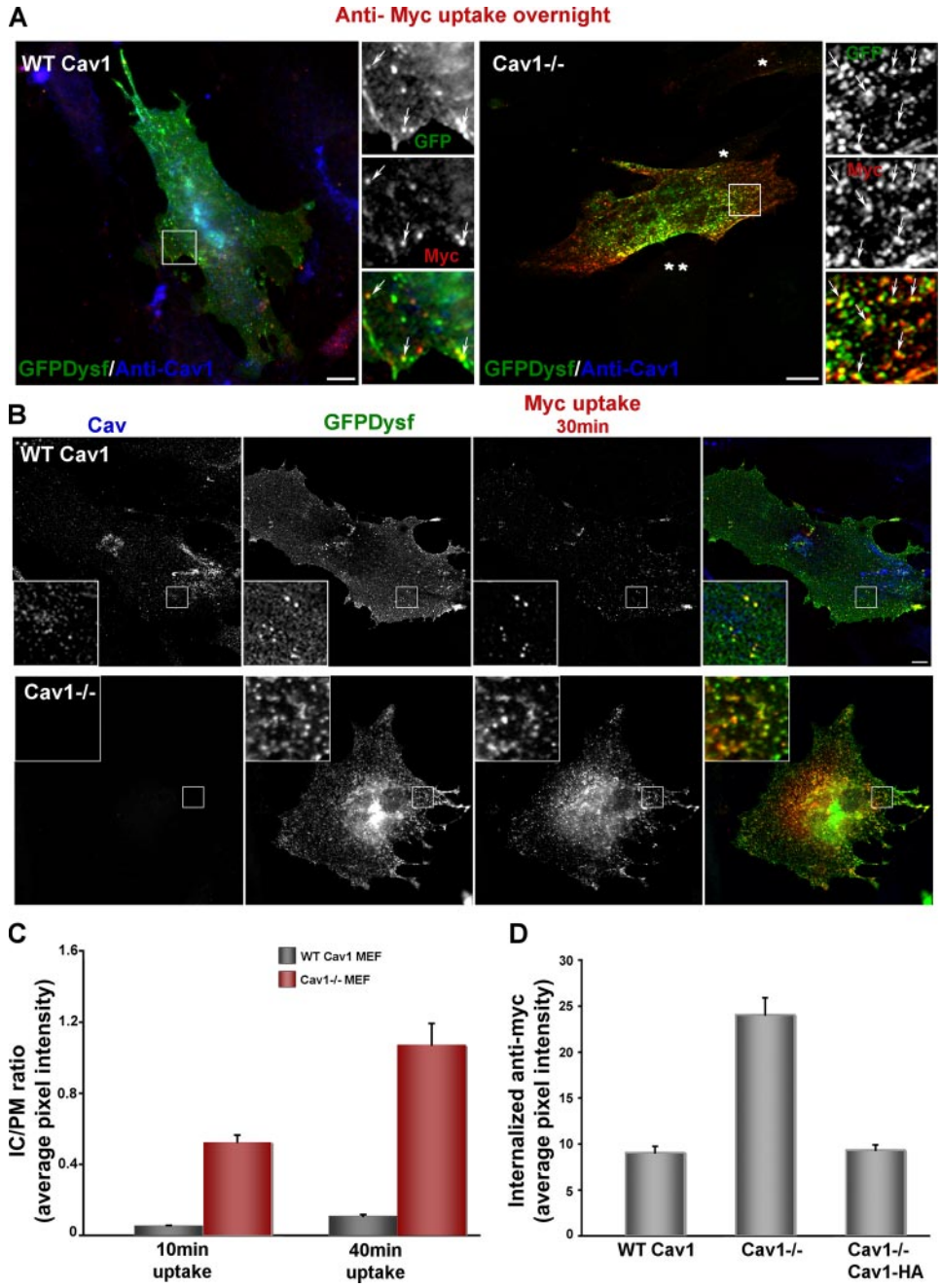

FIGURE 4. **Dysferlin cycles between an intracellular compartment and the plasma membrane.** WT *Cav1* and *Cav1*$^{-/-}$ MEFs were transfected with GFPDysf and allowed to internalized anti-myc antibodies overnight or for 30 min at 37 °C. *A*, in both WT and *Cav1*$^{-/-}$ cells dysferlin is cycling between the PM and an intracellular endocytic compartment. *Inset* shows extensive colocalization between GFPDysf and internalized myc antibodies in *Cav1*$^{-/-}$ cells (*, untransfected cell; **, cell expressing low levels of dysferlin) but in WT *Cav1* cells there is very little internalization. *B*, in WT *Cav1* MEFs dysferlin is mainly localized at the PM although some internalized myc can be seen after 30 min (see *inset*). In contrast after 30 min of myc antibody internalization, dysferlin shows a highly dynamic endocytic traffic in *Cav1*$^{-/-}$ cells; *inset*, extensive overlay between GFPDysf and internalized myc. *C*, time course of myc antibodies uptake in WT or *Cav1*$^{-/-}$ MEFs expressing GFPDysf. The mean fluorescence intensity of dysferlin associated with the PM (myc surface labeling) and internalized myc (2, 10, and 40 min chase at 37 °C) was measured and expressed as IC/PM ratio. *D*, dysferlin internalization is rescued to WT levels by expression of epitope-tagged Cav1 in Cav1$^{-/-}$ MEFs. WT *Cav1* and *Cav1*$^{-/-}$ MEFs were transfected with GFPDysf or co-transfected with GFPDysf and Cav1-HA and anti-myc antibodies were internalized for 20 min at 37 °C. The mean fluorescence intensity of internalized dysferlin (myc labeling) was quantified. *Error bars* are S.E. of three experiments ($n = 30$). *Bars*, 10 μm.

were detected with anti-mouse Alexa Fluor 546 and anti-rabbit Alexa Fluor 647 antibodies after permeabilization. At all time points endocytic vesicles containing myc and GFP antibodies were readily detectable (Fig. 5*A*), demonstrating that internalized dysferlin was targeted to a GPI-AP enriched compartment. We further investigated if dysferlin vesicular traffic followed a dynamin-dependent route using the dynamin inhibitor, Dynasore (57, 58). Whereas transferrin uptake was blocked, dysferlin endocytosis was unaffected by incubation with Dynasore (Fig. 5*B*). We conclude that the major endocytic pathway involved in dysferlin endocytosis in *Cav1*$^{-/-}$ cells is dynamin-independent.

Ultrastructural Analysis of Dysferlin Trafficking—To gain further insights into dysferlin endocytosis, *Cav1*$^{-/-}$ or WT *Cav1* MEFs were transfected with GFP-dysf, then incubated with anti-myc antibodies followed by an anti-mouse HRP-labeled antibody at 4 °C. The cells were then warmed for 2 min at 37 °C, and the DAB reaction visualized in the presence or absence of AA to identify internal structures, as in previous studies (54). The cells were then fixed and processed for correlative light and electron microscopy, identifying GFP-dysf-expressing cells by light microscopy and then sectioning the plastic embedded cells for EM. Consistent with the light microscopy, WT cells showed a uniform, almost continuous, layer of HRP reaction product over the entire cell surface (WT *Cav1* − *AA*; Fig. 6, *A* and *B*) and little internal staining. No preferential staining of caveolae was observed, consistent with our previous immunoelectromicrograph studies (18). In contrast, *Cav1*$^{-/-}$ MEFs showed very patchy sparse labeling over the cell surface (KO − AA; Fig. 6, *C* and *D*) but with some tubular profiles apparently enriched in reaction product (Fig. 6, *E* and *G*). Quantitation of the surface coverage of the HRP reaction product in WT *Cav1* *versus* *Cav1*$^{-/-}$ cells showed a far higher surface coverage in the WT Cav1 cells (see Fig. 6, *A* and *C*) consistent with the low level of surface labeling in *Cav1*$^{-/-}$ cells as observed by light microscopy. Endocytic structures were clearly observed in the *Cav1*$^{-/-}$ cells treated with AA (KO + AA, Fig. 6, *H* and *I*). The ring-shaped morphology and size of the labeled elements are consistent with

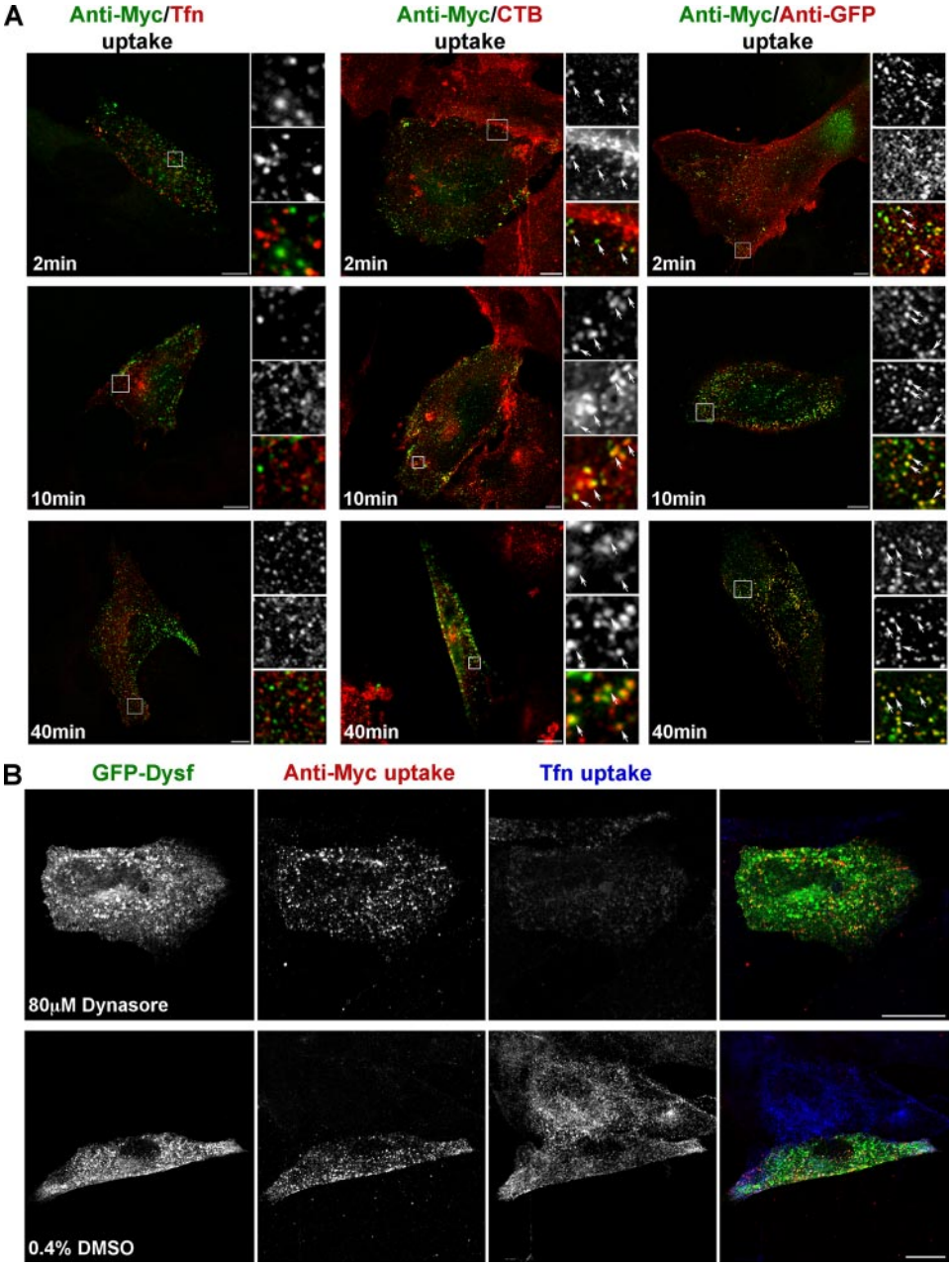

FIGURE 5. **Dysferlin co-internalizes with the early endocytic markers CTB and GPI-AP in a dynamin-independent manner.** *A*, *Cav1*$^{-/-}$ cells were transfected with GFP-dysf or co-transfected with GFP-dysf and TFR or GPI-GFP. Anti-myc antibodies were co-internalized with fluorophore-conjugated Tfn or CTB or anti-GFP antibodies for various times at 37 °C. Dysferlin is internalized mainly via a non-clathrin pathway. No significant colocalization is seen between internalized myc antibodies and Tfn. Dysferlin follows CTB and GPI in their endocytic traffic. Extensive co-internalization is visualized with anti-myc (GFP-dysf) and CTB and GFP (GPI-GFP) after 2, 10, and 40 min uptake. *B*, dynamin inhibitor, Dynasore, does not block dysferlin endocytic traffic. Cav1$^{-/-}$ MEFs were transfected with GFPDysf and incubated in 80 mM Dynasore, 0.4% Me_2SO, Dulbecco's modified Eagle's medium or 0.4% Me_2SO, Dulbecco's modified Eagle's medium alone. Anti-myc antibody or Tfn were internalized for 20 min at 37 °C. Inhibition of dynamin does not block the internalization of anti-myc antibodies by dysferlin, whereas Tfn internalization was blocked. *Bars*, 10 μm (*A*); 20 μm (*B*).

structures labeled by CTB HRP in WT and *Cav1*$^{-/-}$ MEFs in the previous studies (54). These studies show that dysferlin is retained over the entire cell surface in the presence of caveolin but is rapidly internalized in its absence.

Dysferlin Trafficking Is Not Rescued by Caveolin Scaffolding Domain Mutants in Cav1$^{-/-}$ *MEF Cells*—To gain further insights into the functional interaction between dysferlin and caveolin and the relevance of these observations to muscle disease, we examined the effect of caveolin mutants on dysferlin endocytosis as compared with wild type caveolin. We made use of HA-tagged CSD point mutants, Cav3G55S (Cav3G55S-HA) and Cav3C71W (Cav3C71W-HA) (50, 59), which have been linked to muscular dystrophy (11, 13) and the CSD deletion mutant, Cav1Δ81–100 (Cav1Δ-81–100-HA) (60). Quantitation of surface *versus* intracellular dysferlin was performed using antibodies to the lumenal myc tag as in previous studies (18). Cav3G55S-HA or Cav3C71W-HA expressed in *Cav1*$^{-/-}$ MEFs localized predominantly at the surface in a similar fashion to the wild type protein (Fig. 7), whereas Cav1Δ81–100-HA mainly targeted to the Golgi complex as judged by colocalization with the Golgi marker, GM130 (Fig. 7). GFP-dysf was largely localized to intracellular puncta in *Cav1*$^{-/-}$ cells (PM/IC ratio 0.67 ± 0.07) but PM association was restored by re-expression of either Cav1-HA (PM/IC ratio 1.99 ± 0.96) or Cav3-HA (PM/IC ratio 2.3 ± 0.55) (18) (Fig. 8, *A* and *B*). In contrast, expression of Cav1Δ81–100-HA (PM/IC ratio 0.61 ± 0.10), Cav3G55S-HA (PM/IC ratio 0.65 ± 0.15), or Cav3C71W-HA (PM/IC ratio 1.16 ± 0.57) did not affect dysferlin traffic to the PM and dysferlin remained enriched in intracellular vesicles of *Cav1*$^{-/-}$ MEFs (Fig. 8*B*). The lack of an inhibitory effect of these mutants on dysferlin endocytosis is also shown by the uptake of myc antibodies when these mutants are expressed together with GFP-dysf, as compared with the WT Cav3 protein (Fig. 8*C*). The above results suggest that this conserved domain of caveolin is required for inhibition of dysferlin endocytosis and its retention at the PM.

Dominant acting mutants of *Cav3* cause a reduction in surface Cav3, retention of Cav3 in the Golgi complex, and increased degradation (61, 62). We have previously shown that these mutants cause an accumulation of dysferlin in the Golgi complex. We investigated whether this was a result of a block of dysferlin exit from the Golgi rather than a consequence of redistribution due to dysferlin instability at the PM in the

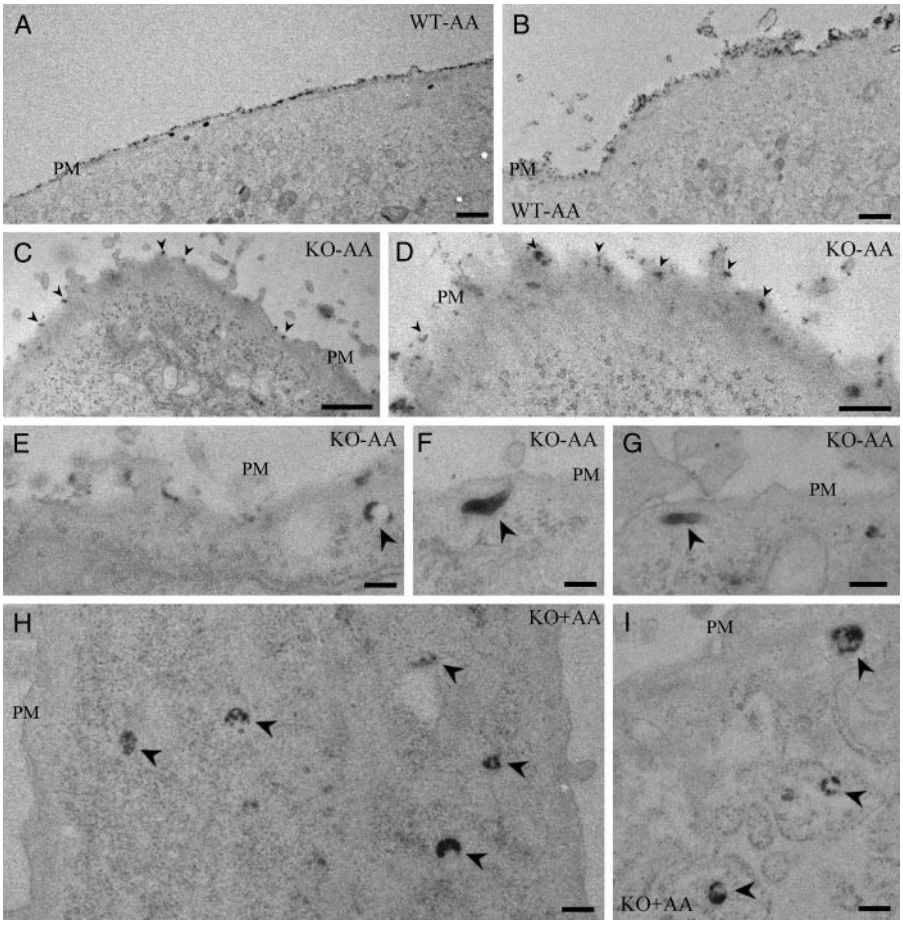

FIGURE 6. **Ultrastructural characterization of dysferlin endocytosis in *Cav1*$^{-/-}$ and WT *Cav1* MEFs.** WT *Cav1* or *Cav1*$^{-/-}$ MEFs were transfected with GFPDysf and then after 14 h were incubated sequentially with antibodies to the lumenal myc tag and then HRP-labeled secondary (anti-mouse) antibodies at 4 °C. The cells were then warmed to 37 °C for 2 min to allow endocytosis to occur. The DAB reaction was performed on the living cells at 4 °C in the presence (+*AA*) or absence (−*AA*) of ascorbic acid as indicated. After fixation the transfected cells were identified under the light microscope by their GFP fluorescence and were marked to allow subsequent identification after embedding in resin. The *marked areas* were sectioned and viewed unstained. In the absence of AA, allowing visualization of both surface and intracellular pools of HRP, WT *Cav1* cells showed HRP reaction product over the entire cell surface (*A* and *B*). In striking contrast, all transfected *Cav1*$^{-/-}$ cells showed sparse patchy surface labeling (*C* and *D*; *arrowheads*) consistent with greatly reduced retention of dysferlin at the plasma membrane. Quantitation of surface coverage by intersection counting (see "Experimental Procedures") showed that 10.3% of the PM of *Cav1*$^{-/-}$ cells was covered in HRP reaction product and 89.0% of the PM of WT cells. Neighboring untransfected cells showed no trace of HRP labeling (results not shown) demonstrating the specificity of the antibody labeling. Potential clathrin-independent early endocytic carriers (*arrowheads*) were frequently observed in the *Cav1*$^{-/-}$ cells (*E–G*). In the presence of ascorbic acid to quench extracellular HRP, internal ring-shaped endocytic elements were clearly demonstrated in the *Cav1*$^{-/-}$ cells (*H* and *I*). *Bars*, *A–D*, 1 μm; *E–I*, 200 nm.

absence of caveolin. No myc antibody uptake was evident in the perinuclear region or intracellular vesicles (Fig. 9*A*) suggesting that dysferlin exit from the Golgi complex was blocked by the dystrophy-associated mutant caveolin and that these mutants have a dominant inhibitory role on Golgi exit. This effect of caveolin-dystrophy mutants on dysferlin exit from the Golgi complex is specific and not a result of their Golgi localization. Expression of a CSD deletion mutant, Cav1Δ81–100, which is also Golgi localized does not restrain dysferlin from exiting the Golgi (Fig. 9*B*). Taken together, these results show two distinct effects of caveolin mutants on trafficking of dysferlin.

DISCUSSION

In this work we have provided novel insights into dysferlin trafficking dynamics with respect to caveolin. Through the use of cells lacking caveolin, by expression of caveolin mutants, and by using different mutants of dysferlin, we have now identified the precise steps in dysferlin trafficking that are regulated by caveolin. We show directly that caveolins can facilitate exit of dysferlin mutants from the Golgi complex. In addition, dominant-acting caveolin mutants inhibit Golgi exit of mutant or wild type dysferlin. However, most unexpectedly, we now show that the primary effect of caveolin is to inhibit dysferlin endocytosis, implicating an endocytic mechanism in caveolin-associated muscle pathology.

Caveolin Modulation of Dysferlin Exit from the Golgi Complex—In cells devoid of caveolin dysferlin accumulates in intracellular vesicular structures, which we now show are endocytic in nature. No accumulation was observed in the Golgi complex and we demonstrated that despite the lack of surface labeling, dysferlin is rapidly transiting the cell surface in these cells, as shown by uptake of extracellular antibodies to a lumenal tag. These results suggest that dysferlin does not absolutely depend on caveolin for Golgi exit. Recent studies have suggested that novel exocytic carriers, containing defined quanta of caveolin, leave the Golgi complex and fuse directly with the PM (63). These carriers, termed exocytic caveolar carriers (64), form a novel exocytic pathway distinct from classical exocytic carriers (see scheme in Fig. 10); these carriers would presumably be absent in cells lacking caveolin. Our data provide new insights into these pathways. Full-length dysferlin can clearly utilize a non-caveolar carrier pathway to reach the PM, as shown in *Cav1*$^{-/-}$ cells. Similarly, a dysferlin mutant lacking all six C2 domains (Δ-C2) can also efficiently reach the PM, both in the absence or presence of caveolin again showing use of a non-caveolar carrier. However, in stark contrast to these two constructs, a protein of intermediate length, which lacks four C2 domains, shows an absolute dependence on caveolin for exit from the Golgi complex (Fig. 2 and scheme in Fig. 10). Whereas this is an artificially generated construct, these results clearly demonstrate a role for caveolin in Golgi exit, as suggested previously for a number of proteins including the angiotensin receptor (59), insulin receptor (65), and the stretch-activated channel, TRPC1 (66). The structural features that make these proteins dependent on caveolin for Golgi exit

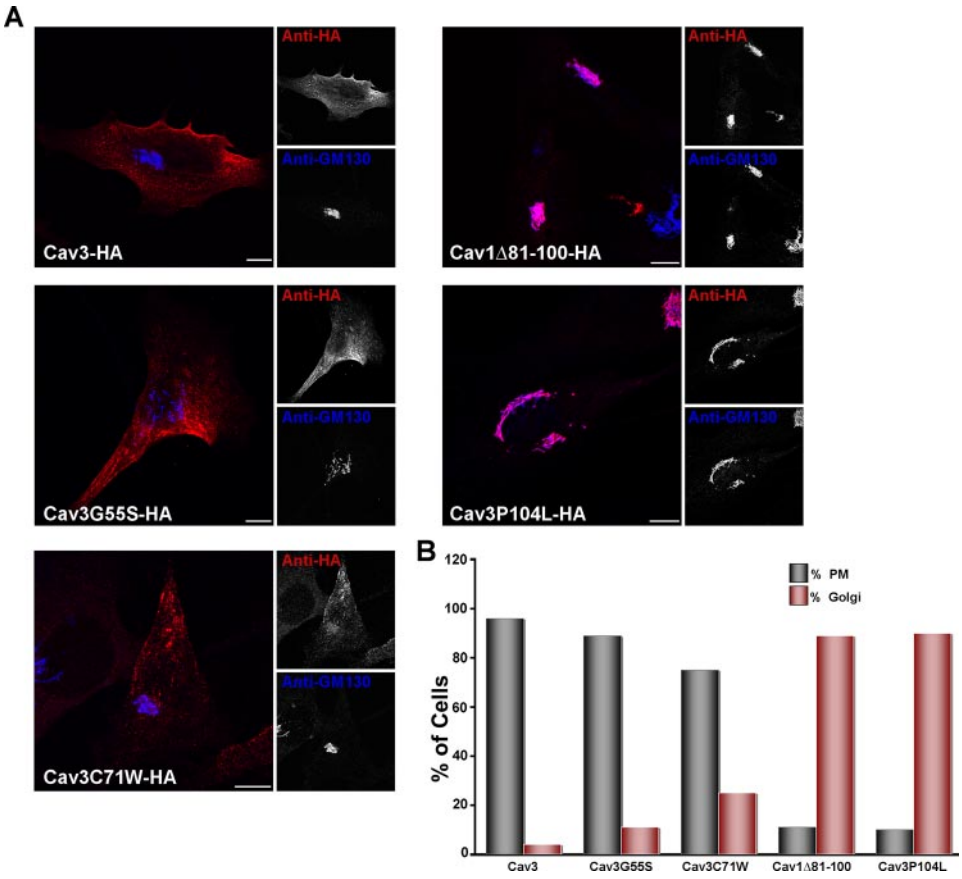

FIGURE 7. **Subcellular distribution of caveolin scaffolding domain mutants.** *Cav1*$^{-/-}$ cells were transfected with HA-tagged Cav3, Cav3G55S, Cav3C71W, Cav1Δ81–100, and Cav3P104L, and colabeled with anti-HA and anti-GM130 antibodies. *A*, similarly to the wild type Cav3, the CSD mutants Cav3G55S and Cav3C71W CSD are targeted to the PM. In contrast, deletion of the CSD, Cav1Δ81–100, results in accumulation in the Golgi complex similarly to the dystrophy mutant Cav3P104L, demonstrated by the extensive overlap with the Golgi marker, GM130. *B*, CSD mutant predominant phenotypes were scored based on colabeling with relevant intracellular markers. Results are presented as percentage of cells showing a prevalent subcellular localization, and are representative of three individual experiments (n = 30–250/for each construct). *Bar*, 10 μm.

are as yet, unclear. In the case of dysferlin, it appears that the shorter construct is absolutely dependent on the caveolar pathway, whereas the additional cytoplasmic region of the full-length protein allows the protein to use multiple pathways. This might involve interaction of the terminal C2 domains with cellular machinery involved in trafficking via these caveolin-independent pathways. One candidate protein is Ahnak, which interacts with the C2A domain of dysferlin (67). Ahnak is a marker of a distinct exocytic vesicle, the enlargeosome (68, 69). Consistent with a role for dysferlin in membrane repair (24), enlargeosomes are proposed to be the source of membrane during PM resealing (68). Although enlargeosomes do not associate with caveolin-enriched detergent-resistant membranes (69) it remains to be examined whether dysferlin exits the Golgi via enlargeosomes. As C2 domains have also been implicated in phospholipid binding it is also possible that interaction with the distinct domains of the Golgi membrane allow segregation of dysferlin away from the caveolar domain.

Dystrophy Mutants of Caveolin Disrupt Golgi Exit of Both Full-length Dysferlin and Dysferlin Truncation Mutants—We have previously demonstrated that dystrophy-associated mutants of caveolin (Cav3P104L and Cav3R26Q) cause dysferlin accumulation within the Golgi complex (18). We find no evidence for dysferlin transport to the cell surface under these conditions suggesting that the caveolin mutants cause a complete block in Golgi exit. Interestingly, this was true for all the tested membrane-associated dysferlin constructs, including Δ-C2, which lacks most of the cytoplasmic domain and traffics to the PM in a caveolin-independent manner. This raises the possibility that mutant caveolin might perturb dysferlin trafficking at an earlier stage in the Golgi complex, before divergence of the two pathways. Consistent with this, Golgi caveolin mutants accumulate throughout the Golgi complex including the cis Golgi (18, 47). The specificity of this effect is shown by the fact that a Golgi-localized form of caveolin lacking amino acids 81–100 does not prevent dysferlin from exiting the Golgi. This suggests that a direct interaction between dysferlin and caveolin, at least, at the Golgi level may be taking place. If so, this narrows down the interacting domain of dysferlin to the TM domain and nearby cytoplasmic region, which contains four potential CSD binding motifs. However, these findings do not rule out perturbation of lipid domains of the Golgi complex, which may be influenced by expression of a form of caveolin with mutations in this potential lipid-binding domain (45). If so, these effects are restricted to specific cargo proteins as the transit of other proteins, such as GPI-anchored proteins, through the Golgi complex is unaffected by the expression of the mutant caveolin proteins (18).

Caveolins Inhibit Dysferlin Endocytosis—We show here for the first time that caveolins inhibit endocytosis of dysferlin. In cells lacking Cav1 and Cav3, dysferlin is rapidly cleared from the PM resulting in a low level of PM dysferlin in contrast to a large intracellular pool at steady state. Our results show a much higher endocytic rate for dysferlin in *Cav1*$^{-/-}$ cells as antibodies to a lumenal tag accumulate far more rapidly in *Cav1*$^{-/-}$ cells than in cells expressing Cav1 or Cav3 despite the higher level of surface dysferlin in these cells (see Figs. 4 and 8) (18). Expression of *Cav1* or *Cav3*, but not specific caveolin mutants, inhibits dysferlin endocytosis resulting in its retention at the cell surface and a high level of PM dysferlin. Dysferlin endocytosis in *Cav1*$^{-/-}$ cells is via a dynamin (and caveolin-)-independent pathway. Colocalization with GPI-anchored proteins and CTB, but not transferrin, at early stages of endocytosis strongly implicates the CLIC/GEEC clathrin-independent pathway (54, 56) in dysferlin endocytosis. This is supported by

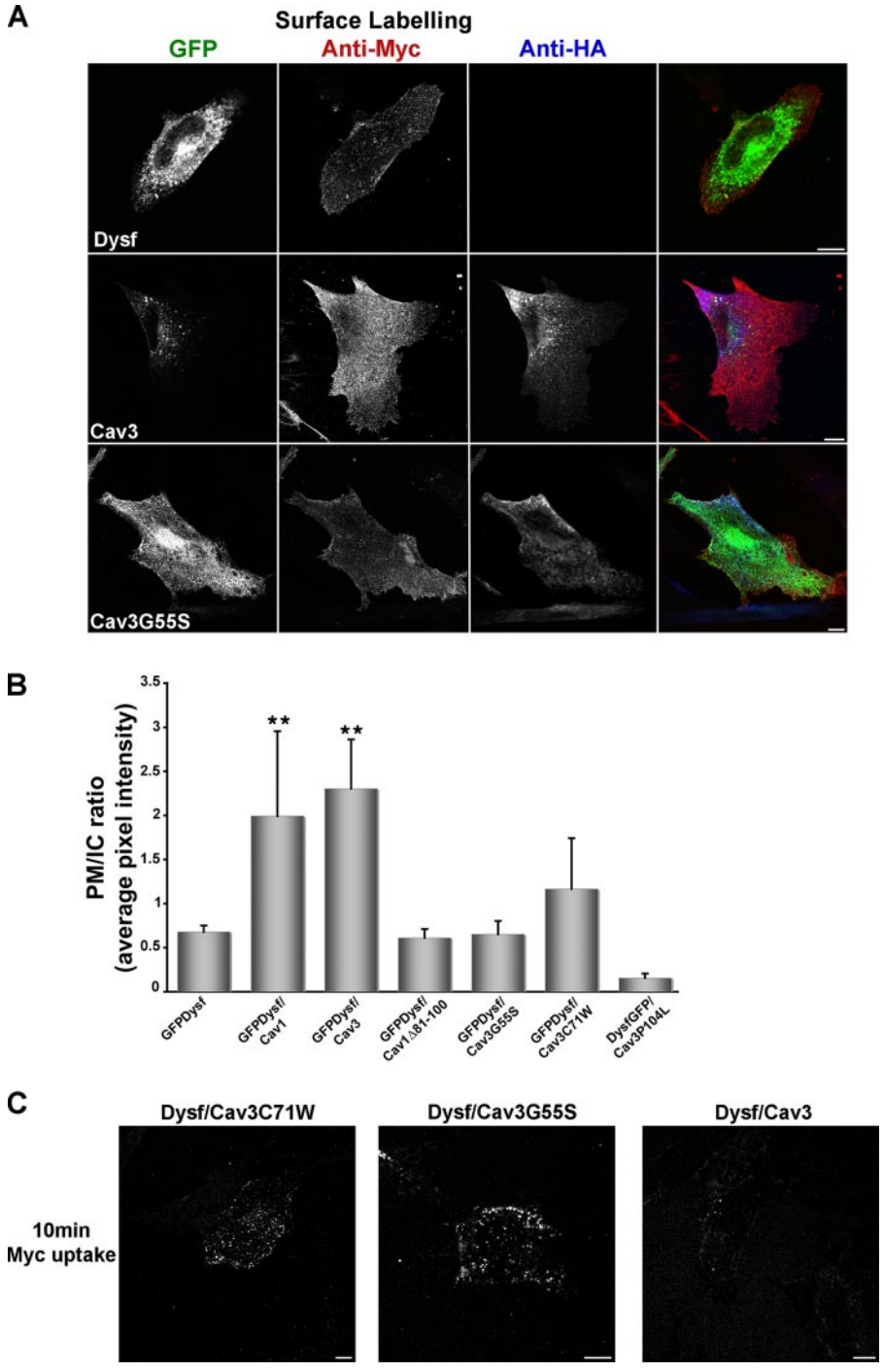

FIGURE 8. **Dysferlin retention at the PM is dependent on an intact CSD.** Expression of CSD point mutants does not rescue dysferlin traffic to the PM in *Cav1*$^{-/-}$ MEF cells. *Cav1*$^{-/-}$ cells were transfected with GFPDysf or co-transfected with GFPDysf and HA-tagged Cav3, Cav3G55S, Cav3C71W, Cav1Δ81–100, and Cav3P104L and labeled with rabbit anti-HA and mouse anti-myc antibodies. Surface labeling of dysferlin and quantification of PM and intracellular pools of dysferlin were performed as described under "Experimental Procedures." *A*, in cells lacking caveolin dysferlin is mainly targeted to intracellular puncta throughout the cytoplasm. Whereas expression of epitope-tagged Cav3 rescues dysferlin traffic to the PM, expression of CSD mutants (*i.e.* Cav3G55S) does not rescue dysferlin traffic to the PM. *B*, the mean fluorescence intensity of dysferlin associated with the PM (myc labeling) and intracellular structures (GFP labeling) was measured and expressed as the PM/IC ratio. *Error bars* are S.E. of three experiments ($n = 30$); **, $p < 0.001$. *C*, *Cav1*$^{-/-}$ cells co-expressing *GFPDysf* and HA-tagged, Cav3C71W, Cav3G55S, or Cav3 were allowed to uptake anti-myc antibodies for 10 min at 37 °C. Expression of Cav3C71W or Cav3G55S, but not WT Cav3 protein, have no effect on dysferlin endocytosis as demonstrated by the internalization of anti-myc antibodies. *Bars*, 10 μm.

ultrastructural analysis of the endocytic pathway showing dysferlin in tubular/ring-shaped early endosomal elements. These results suggest a novel role of this pathway in regulating dysferlin surface expression and, a role for caveolin in inhibiting the clathrin-independent endocytosis of specific markers.

The inhibitory effect of caveolins on dysferlin endocytosis presents an interesting conundrum. We believe that a direct inhibitory effect of caveolin by binding dysferlin to immobile caveolar domains is unlikely; both electron microscopy and light microscopy show that dysferlin does not colocalize significantly with caveolin, even at the level of light microscopy, and both immuno-EM on frozen sections (18) and EM surface labeling experiments (this study) confirmed that dysferlin was not concentrated within caveolae. Thus, the inhibition by caveolin appears to be indirect. Yet our results suggest that the effect of caveolin on dysferlin endocytosis is specific; whereas acute Cav1 expression has been shown to inhibit clathrin-independent endocytosis of CTB (54, 70) and SV40 is efficiently internalized by cells devoid of caveolae (71) CTB and SV40 internalization was quantitatively identical in WT *Cav1* and *Cav1*$^{-/-}$ MEFs as used here. Furthermore, no effect on GPI-AP internalization could be detected in *Cav1*$^{-/-}$ cells. This argues against a general negative inhibitory role of caveolins on clathrin-independent endocytosis, but suggests that caveolins specifically inhibit dysferlin entry into this pathway. We could also show that the increased uptake of dysferlin in *Cav1*$^{-/-}$ cells was not due to increased endocytosis caused by dysferlin expression (results not shown). Caveolae have been suggested to be negative regulators of clathrin-independent endocytosis (70, 72) but other work identifies caveolae as endocytic vehicles (73–75). A new concept described here is that caveolin is regulating the non-caveolar endocytosis of dysferlin as we have

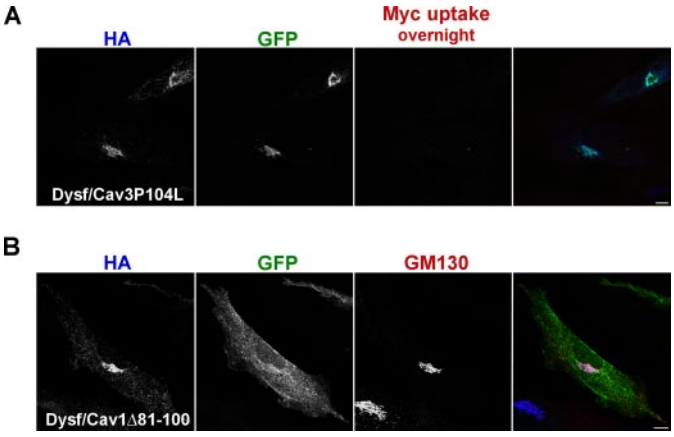

FIGURE 9. **Dystrophy mutant of Cav3 has a dominant inhibitory effect on dysferlin exit from the Golgi.** *Cav1*$^{-/-}$ cells were co-transfected with GFP-Dysf and HA-tagged Cav3P104L or Cav1Δ81–100 and labeled with rabbit anti-HA (*A* and *B*) and mouse anti-GM130 (*B*) antibodies. Anti-myc antibody was internalized overnight (*B*). *A*, expression of Cav3P04L-HA blocks dysferlin exit from the Golgi apparatus. No significant Golgi pool of internalized myc antibodies is seen after overnight incubation at 37 °C. *B*, expression of Golgi-localized epitope-tagged Cav1Δ81–100 mutant does not affect GFP-dysf exit from the Golgi apparatus. Cav1Δ81–100, but not GFPDysf, is retained in the Golgi complex as demonstrated by colocalization with the Golgi marker, GM130. *Bars*, 10 μm.

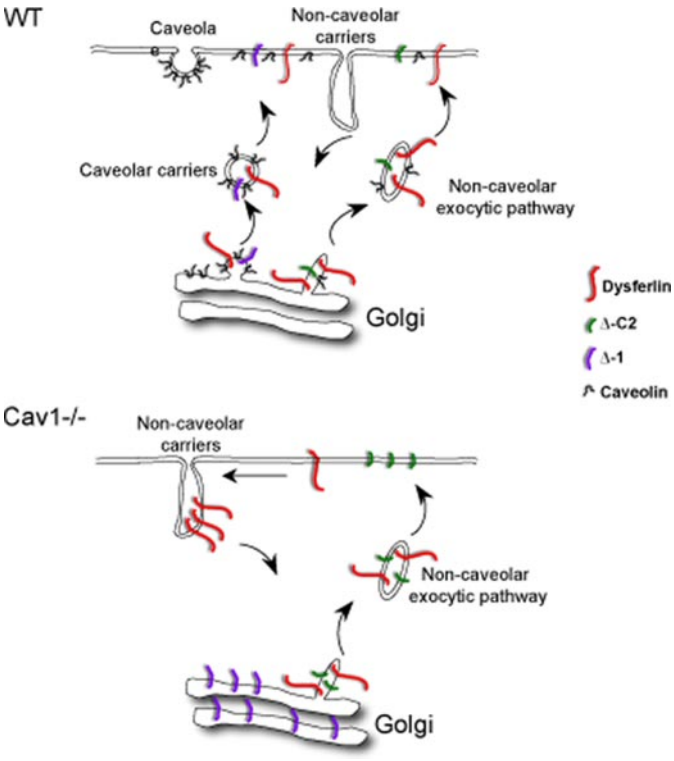

FIGURE 10. **Model for regulation of caveolin trafficking by caveolin.** In WT *Cav1* cells full-length dysferlin exit from the Golgi complex may take place via caveolar and noncaveolar exocytic carriers. In *Cav1*$^{-/-}$ cells dysferlin must use an alternative pathway(s). However, a truncation mutant lacking part of the cytoplasmic domain (Δ-1) is completely dependent on caveolin for Golgi exit as it cannot enter the non-caveolar pathway. A more severe mutant (Δ-C2) traffics to the PM in a caveolin-independent manner as it lacks information for incorporation into caveolar carriers. Retention of dysferlin at the PM is dependent on caveolin/caveolae due to inhibition of dysferlin endocytosis by caveolin. A truncation of dysferlin lacking all six C2 domains, Δ-C2, is not internalized suggesting a role for the cytoplasmic domain in endocytosis.

clearly demonstrated that dysferlin is not concentrated in caveolae.

A model for the inhibitory effect of caveolin on endocytosis must take into account the intriguing finding that two *Cav3* single point mutants, which occur naturally in the human population, did not inhibit dysferlin endocytosis in complete contrast to the wild type protein. This implicates the scaffolding domain of caveolin in its inhibitory activity. The two inhibitory mutants were initially reported as dystrophy mutants (11) but subsequently have been shown to occur as polymorphisms in the population (76, 77). Yet two previous studies have shown specific effects of these mutant proteins in cultured cells (50, 59). Further studies should elucidate the underlying mechanisms involved in the inhibitory activity of the wild type protein in comparison to these single point mutants and whether these mutations can contribute to disease under certain conditions.

In conclusion, these studies have elucidated distinct roles of caveolin in regulating dysferlin trafficking pathways, both in positively regulating exocytosis and negatively regulating endocytosis via a clathrin-independent pathway for which dysferlin acts as a new marker. An interesting possibility is that this inhibitory activity of caveolin on endocytosis is regulated *in vivo*, allowing modulation of the surface levels of dysferlin and membrane remodeling. Whether caveolin acts in a similar fashion on other surface proteins will require further investigation. The involvement of endocytosis in muscle disease may be a more general phenomenon. Another sarcolemmal protein, α-sarcoglycan, which is linked to a subset of muscle disease limb girdle muscular dystrophy 2D (78, 79), is translocated from the cell surface to endosomes upon perturbation of its PM stability (80). α-Sarcoglycan stability at the PM relies on a proper assembly of the sarcoglycan complex (80). Thus dysferlin and α-sarcoglycan represent examples of sarcolemmal proteins where endocytic mechanisms play a central role in maintaining the integrity of the PM.

These results provide new insights into the functions of caveolins and the mechanisms underlying caveolin-related diseases. In addition, they provide fundamental insights into the regulation of exocytic and endocytic trafficking pathways of membrane proteins in mammalian cells and the importance of this poorly characterized clathrin-independent endocytic pathway in surface remodeling of specific PM components.

Acknowledgments—We thank Michelle Hill for preparation of immortalized mouse embryonic fibroblast cell lines and Rachel Hancock for technical assistance in EM processing. We also thank members of the Parton group for critical reading of the manuscript. Confocal microscopy was performed at the ACRF/IMB Dynamic Imaging Facility for Cancer Biology, established with funding from the Australian Cancer Research Foundation. The Institute for Molecular Bioscience is a Special Research Centre of the Australian Research Council.

REFERENCES

1. Aoki, M., Liu, J., Richard, I., Bashir, R., Britton, S., Keers, S. M., Oeltjen, J., Brown, H. E., Marchand, S., Bourg, N., Beley, C., McKenna-Yasek, D., Arahata, K., Bohlega, S., Cupler, E., Illa, I., Majneh, I., Barohn, R. J., Urtizberea, J. A., Fardeau, M., Amato, A., Angelini, C., Bushby, K., Beckmann,

J. S., and Brown, R. H., Jr. (2001) *Neurology* **57,** 271–278
2. Bashir, R., Britton, S., Strachan, T., Keers, S., Vafiadaki, E., Lako, M., Richard, I., Marchand, S., Bourg, N., Argov, Z., Sadeh, M., Mahjneh, I., Marconi, G., Passos-Bueno, M. R., Moreira Ede, S., Zatz, M., Beckmann, J. S., and Bushby, K. (1998) *Nat. Genet.* **20,** 37–42
3. Illa, I., Serrano-Munuera, C., Gallardo, E., Lasa, A., Rojas-Garcia, R., Palmer, J., Gallano, P., Baiget, M., Matsuda, C., and Brown, R. H. (2001) *Ann. Neurol.* **49,** 130–134
4. Liu, J., Aoki, M., Illa, I., Wu, C., Fardeau, M., Angelini, C., Serrano, C., Urtizberea, J. A., Hentati, F., Hamida, M. B., Bohlega, S., Culper, E. J., Amato, A. A., Bossie, K., Oeltjen, J., Bejaoui, K., McKenna-Yasek, D., Hosler, B. A., Schurr, E., Arahata, K., de Jong, P. J., and Brown, R. H., Jr. (1998) *Nat. Genet.* **20,** 31–36
5. Matsuda, C., Aoki, M., Hayashi, Y. K., Ho, M. F., Arahata, K., and Brown, R. H., Jr. (1999) *Neurology* **53,** 1119–1122
6. Betz, R. C., Schoser, B. G., Kasper, D., Ricker, K., Ramirez, A., Stein, V., Torbergsen, T., Lee, Y. A., Nothen, M. M., Wienker, T. F., Malin, J. P., Propping, P., Reis, A., Mortier, W., Jentsch, T. J., Vorgerd, M., and Kubisch, C. (2001) *Nat. Genet.* **28,** 218–219
7. Carbone, I., Bruno, C., Sotgia, F., Bado, M., Broda, P., Masetti, E., Panella, A., Zara, F., Bricarelli, F. D., Cordone, G., Lisanti, M. P., and Minetti, C. (2000) *Neurology* **54,** 1373–1376
8. Figarella-Branger, D., Pouget, J., Bernard, R., Krahn, M., Fernandez, C., Levy, N., and Pellissier, J. F. (2003) *Neurology* **61,** 562–564
9. Fischer, D., Schroers, A., Blumcke, I., Urbach, H., Zerres, K., Mortier, W., Vorgerd, M., and Schroder, R. (2003) *Ann. Neurol.* **53,** 233–241
10. Kubisch, C., Schoser, B. G., von During, M., Betz, R. C., Goebel, H. H., Zahn, S., Ehrbrecht, A., Aasly, J., Schroers, A., Popovic, N., Lochmuller, H., Schroder, J. M., Bruning, T., Malin, J. P., Fricke, B., Meinck, H. M., Torbergsen, T., Engels, H., Voss, B., and Vorgerd, M. (2003) *Ann. Neurol.* **53,** 512–520
11. McNally, E. M., de Sa Moreira, E., Duggan, D. J., Bonnemann, C. G., Lisanti, M. P., Lidov, H. G., Vainzof, M., Passos-Bueno, M. R., Hoffman, E. P., Zatz, M., and Kunkel, L. M. (1998) *Hum. Mol. Genet.* **7,** 871–877
12. Merlini, L., Carbone, I., Capanni, C., Sabatelli, P., Tortorelli, S., Sotgia, F., Lisanti, M. P., Bruno, C., and Minetti, C. (2002) *J. Neurol. Neurosurg. Psychiatry* **73,** 65–67
13. Minetti, C., Sotgia, F., Bruno, C., Scartezzini, P., Broda, P., Bado, M., Masetti, E., Mazzocco, M., Egeo, A., Donati, M. A., Volonte, D., Galbiati, F., Cordone, G., Bricarelli, F. D., Lisanti, M. P., and Zara, F. (1998) *Nat. Genet.* **18,** 365–368
14. Tateyama, M., Aoki, M., Nishino, I., Hayashi, Y. K., Sekiguchi, S., Shiga, Y., Takahashi, T., Onodera, Y., Haginoya, K., Kobayashi, K., Iinuma, K., Nonaka, I., Arahata, K., Itoyama, Y., and Itoyoma, Y. (2002) *Neurology* **58,** 323–325
15. Vorgerd, M., Ricker, K., Ziemssen, F., Kress, W., Goebel, H. H., Nix, W. A., Kubisch, C., Schoser, B. G., and Mortier, W. (2001) *Neurology* **57,** 2273–2277
16. Capanni, C., Sabatelli, P., Mattioli, E., Ognibene, A., Columbaro, M., Lattanzi, G., Merlini, L., Minetti, C., Maraldi, N. M., and Squarzoni, S. (2003) *Exp. Mol. Med.* **35,** 538–544
17. Matsuda, C., Hayashi, Y. K., Ogawa, M., Aoki, M., Murayama, K., Nishino, I., Nonaka, I., Arahata, K., and Brown, R. H., Jr. (2001) *Hum. Mol. Genet.* **10,** 1761–1766
18. Hernandez-Deviez, D. J., Martin, S., Laval, S. H., Lo, H. P., Cooper, S. T., North, K. N., Bushby, K., and Parton, R. G. (2006) *Hum. Mol. Genet.* **15,** 129–142
19. Yabe, I., Kawashima, A., Kikuchi, S., Higashi, T., Fukazawa, T., Hamada, T., Sasaki, H., and Tashiro, K. (2003) *Acta Neurol. Scand.* **108,** 47–51
20. Britton, S., Freeman, T., Vafiadaki, E., Keers, S., Harrison, R., Bushby, K., and Bashir, R. (2000) *Genomics* **68,** 313–321
21. Davis, D. B., Delmonte, A. J., Ly, C. T., and McNally, E. M. (2000) *Hum. Mol. Genet.* **9,** 217–226
22. Yasunaga, S., Grati, M., Cohen-Salmon, M., El-Amraoui, A., Mustapha, M., Salem, N., El-Zir, E., Loiselet, J., and Petit, C. (1999) *Nat. Genet.* **21,** 363–369
23. Weiler, T., Bashir, R., Anderson, L. V., Davison, K., Moss, J. A., Britton, S., Nylen, E., Keers, S., Vafiadaki, E., Greenberg, C. R., Bushby, C. R., and Wrogemann, K. (1999) *Hum. Mol. Genet.* **8,** 871–877
24. Bansal, D., and Campbell, K. P. (2004) *Trends Cell Biol.* **14,** 206–213
25. Bansal, D., Miyake, K., Vogel, S. S., Groh, S., Chen, C. C., Williamson, R., McNeil, P. L., and Campbell, K. P. (2003) *Nature* **423,** 168–172
26. Mikoshiba, K., Fukuda, M., Ibata, K., Kabayama, H., and Mizutani, A. (1999) *Chem. Phys. Lipids* **98,** 59–67
27. Nalefski, E. A., and Falke, J. J. (1996) *Protein Sci.* **5,** 2375–2390
28. Pallanck, L. (2003) *Trends Neurosci.* **26,** 2–4
29. Rizo, J., and Sudhof, T. C. (1998) *J. Biol. Chem.* **273,** 15879–15882
30. Rothberg, K. G., Heuser, J. E., Donzell, W. C., Ying, Y. S., Glenney, J. R., and Anderson, R. G. (1992) *Cell* **68,** 673–682
31. Scherer, P. E., Lewis, R. Y., Volonte, D., Engelman, J. A., Galbiati, F., Couet, J., Kohtz, D. S., van Donselaar, E., Peters, P., and Lisanti, M. P. (1997) *J. Biol. Chem.* **272,** 29337–29346
32. Tang, Z., Scherer, P. E., Okamoto, T., Song, K., Chu, C., Kohtz, D. S., Nishimoto, I., Lodish, H. F., and Lisanti, M. P. (1996) *J. Biol. Chem.* **271,** 2255–2261
33. Way, M., and Parton, R. G. (1995) *FEBS Lett.* **376,** 108–112
34. Kurzchalia, T. V., Dupree, P., Parton, R. G., Kellner, R., Virta, H., Lehnert, M., and Simons, K. (1992) *J. Cell Biol.* **118,** 1003–1014
35. Williams, T. M., and Lisanti, M. P. (2004) *Genome Biol.* **5,** 214
36. Doyle, D. D., Upshaw-Earley, J., Bell, E., and Palfrey, H. C. (2003) *Biochem. Biophys. Res. Commun.* **304,** 22–25
37. Song, K. S., Scherer, P. E., Tang, Z., Okamoto, T., Li, S., Chafel, M., Chu, C., Kohtz, D. S., and Lisanti, M. P. (1996) *J. Biol. Chem.* **271,** 15160–15165
38. Ikonen, E., Heino, S., and Lusa, S. (2004) *Biochem. Soc. Trans.* **32,** 121–123
39. Razani, B., Schlegel, A., and Lisanti, M. P. (2000) *J. Cell Sci.* **113**, 2103–2109
40. Cheng, Z. J., Singh, R. D., Marks, D. L., and Pagano, R. E. (2006) *Mol. Membr. Biol.* **23,** 101–110
41. Parton, R. G., and Richards, A. A. (2003) *Traffic* **4,** 724–738
42. Nichols, B. (2003) *J. Cell Sci.* **116,** 4707–4714
43. Dupree, P., Parton, R. G., Raposo, G., Kurzchalia, T. V., and Simons, K. (1993) *EMBO J.* **12,** 1597–1605
44. Monier, S., Parton, R. G., Vogel, F., Behlke, J., Henske, A., and Kurzchalia, T. V. (1995) *Mol. Biol. Cell* **6,** 911–927
45. Parton, R. G., Hanzal-Bayer, M., and Hancock, J. F. (2006) *J. Cell Sci.* **119,** 787–796
46. Couet, J., Li, S., Okamoto, T., Ikezu, T., and Lisanti, M. P. (1997) *J. Biol. Chem.* **272,** 6525–6533
47. Luetterforst, R., Stang, E., Zorzi, N., Carozzi, A., Way, M., and Parton, R. G. (1999) *J. Cell Biol.* **145,** 1443–1459
48. Prior, I. A., Harding, A., Yan, J., Sluimer, J., Parton, R. G., and Hancock, J. F. (2001) *Nat. Cell Biol.* **3,** 368–375
49. Klinge, L., Laval, S., Keers, S., Haldane, F., Straub, V., Barresi, R., and Bushby, K. (2007) *FASEB J.* **21,** 1768–1776
50. Carozzi, A. J., Roy, S., Morrow, I. C., Pol, A., Wyse, B., Clyde-Smith, J., Prior, I. A., Nixon, S. J., Hancock, J. F., and Parton, R. G. (2002) *J. Biol. Chem.* **277,** 17944–17949
51. Morrow, I. C., Rea, S., Martin, S., Prior, I. A., Prohaska, R., Hancock, J. F., James, D. E., and Parton, R. G. (2002) *J. Biol. Chem.* **277,** 48834–48841
52. Razani, B., Engelman, J. A., Wang, X. B., Schubert, W., Zhang, X. L., Marks, C. B., Macaluso, F., Russell, R. G., Li, M., Pestell, R. G., Di Vizio, D., Hou, H., Jr., Kneitz, B., Lagaud, G., Christ, G. J., Edelmann, W., and Lisanti, M. P. (2001) *J. Biol. Chem.* **276,** 38121–38138
53. Sotgia, F., Razani, B., Bonuccelli, G., Schubert, W., Battista, M., Lee, H., Capozza, F., Schubert, A. L., Minetti, C., Buckley, J. T., and Lisanti, M. P. (2002) *Mol. Cell. Biol.* **22,** 3905–3926
54. Kirkham, M., Fujita, A., Chadda, R., Nixon, S. J., Kurzchalia, T. V., Sharma, D. K., Pagano, R. E., Hancock, J. F., Mayor, S., and Parton, R. G. (2005) *J. Cell Biol.* **168,** 465–476
55. Naslavsky, N., Weigert, R., and Donaldson, J. G. (2004) *Mol. Biol. Cell* **15,** 3542–3552
56. Sabharanjak, S., Sharma, P., Parton, R. G., and Mayor, S. (2002) *Dev. Cell* **2,** 411–423
57. Macia, E., Ehrlich, M., Massol, R., Boucrot, E., Brunner, C., and Kirchhausen, T. (2006) *Dev. Cell* **10,** 839–850
58. Newton, A. J., Kirchhausen, T., and Murthy, V. N. (2006) *Proc. Natl. Acad. Sci. U. S. A.* **103,** 17955–17960

59. Wyse, B. D., Prior, I. A., Qian, H., Morrow, I. C., Nixon, S., Muncke, C., Kurzchalia, T. V., Thomas, W. G., Parton, R. G., and Hancock, J. F. (2003) *J. Biol. Chem.* **278,** 23738–23746
60. Ren, X., Ostermeyer, A. G., Ramcharan, L. T., Zeng, Y., Lublin, D. M., and Brown, D. A. (2004) *Mol. Biol. Cell* **15,** 4556–4567
61. Sotgia, F., Woodman, S. E., Bonuccelli, G., Capozza, F., Minetti, C., Scherer, P. E., and Lisanti, M. P. (2003) *Am. J. Physiol.* **285,** C1150–C1160
62. Galbiati, F., Volonte, D., Minetti, C., Chu, J. B., and Lisanti, M. P. (1999) *J. Biol. Chem.* **274,** 25632–25641
63. Tagawa, A., Mezzacasa, A., Hayer, A., Longatti, A., Pelkmans, L., and Helenius, A. (2005) *J. Cell Biol.* **170,** 769–779
64. Parton, R. G., and Simons, K. (2007) *Nat. Rev.* **8,** 185–194
65. Cohen, A. W., Razani, B., Wang, X. B., Combs, T. P., Williams, T. M., Scherer, P. E., and Lisanti, M. P. (2003) *Am. J. Physiol.* **285,** C222–C235
66. Brazer, S. C., Singh, B. B., Liu, X., Swaim, W., and Ambudkar, I. S. (2003) *J. Biol. Chem.* **278,** 27208–27215
67. Huang, Y., Laval, S. H., van Remoortere, A., Baudier, J., Benaud, C., Anderson, L. V., Straub, V., Deelder, A., Frants, R. R., den Dunnen, J. T., Bushby, K., and van der Maarel, S. M. (2007) *FASEB J.* **21,** 732–742
68. Borgonovo, B., Cocucci, E., Racchetti, G., Podini, P., Bachi, A., and Meldolesi, J. (2002) *Nat. Cell Biol.* **4,** 955–962
69. Cocucci, E., Racchetti, G., Podini, P., Rupnik, M., and Meldolesi, J. (2004) *Mol. Biol. Cell* **15,** 5356–5368
70. Le, P. U., Guay, G., Altschuler, Y., and Nabi, I. R. (2002) *J. Biol. Chem.* **277,** 3371–3379
71. Damm, E. M., Pelkmans, L., Kartenbeck, J., Mezzacasa, A., Kurzchalia, T., and Helenius, A. (2005) *J. Cell Biol.* **168,** 477–488
72. Nabi, I. R., and Le, P. U. (2003) *J. Cell Biol.* **161,** 673–677
73. Sharma, D. K., Brown, J. C., Choudhury, A., Peterson, T. E., Holicky, E., Marks, D. L., Simari, R., Parton, R. G., and Pagano, R. E. (2004) *Mol. Biol. Cell* **15,** 3114–3122
74. Di Guglielmo, G. M., Le Roy, C., Goodfellow, A. F., and Wrana, J. L. (2003) *Nat. Cell Biol.* **5,** 410–421
75. Pelkmans, L., Kartenbeck, J., and Helenius, A. (2001) *Nat. Cell Biol.* **3,** 473–483
76. de Paula, F., Vainzof, M., Bernardino, A. L., McNally, E., Kunkel, L. M., and Zatz, M. (2001) *Am. J. Med. Genet.* **99,** 303–307
77. Vatta, M., Ackerman, M. J., Ye, B., Makielski, J. C., Ughanze, E. E., Taylor, E. W., Tester, D. J., Balijepalli, R. C., Foell, J. D., Li, Z., Kamp, T. J., and Towbin, J. A. (2006) *Circulation* **114,** 2104–2112
78. Fanin, M., Duggan, D. J., Mostacciuolo, M. L., Martinello, F., Freda, M. P., Soraru, G., Trevisan, C. P., Hoffman, E. P., and Angelini, C. (1997) *J. Med. Genet.* **34,** 973–977
79. McNally, E. M., Yoshida, M., Mizuno, Y., Ozawa, E., and Kunkel, L. M. (1994) *Proc. Natl. Acad. Sci. U. S. A.* **91,** 9690–9694
80. Draviam, R. A., Wang, B., Shand, S. H., Xiao, X., and Watkins, S. C. (2006) *Traffic* **7,** 793–810

SUPPLEMENTARY MATERIAL

Figure S1. (A) Dysferlin is not localized to late endosomes in Cav1-/- MEFs. Cav1-/- MEFs expressing GFP-dysf were immunolabeled with markers of the late endosomal/lysosomal compartments. Dysferlin is targeted to an endosomal compartment that is distinct from late-endosomal/lysosomal structures. There is no evident colocalization with LBPA- or LAMP-1 positive compartments.
(B) Expression of Cav1 rescues dysferlin endocytic phenotype in Cav1-/- MEFs. WT Cav1 and Cav1-/- MEFs were transfected with GFP-dysf or co-transfected with GFP-dysf and Cav1-HA and anti-myc antibodies were internalized for 20 min at 37ºC. Cells were labeled with antibodies against endogenous caveolin or the HA tag. Dysferlin internalization is rescued to WT levels by expression of HA-tagged Cav1 in Cav1-/- MEFs. Very few punctate structures colabeled with GFP-dysf. Internalised anti-myc antibodies are seen in WT or Cav1-/- MEFs expressing GFP-dysf or coexpressing GFP-dysf and Cav1-HA, respectively. In contrast, Cav1-/- MEFs expressing GFP-dysf alone show extensive overlap with internalised anti-myc.
(C) WT and Cav1-/- MEFs have similar endocytic rates. WT Cav1 and Cav1-/- MEFs were allowed to internalise Tfn or CTB for 10min at 37ºC. There is no significant difference in the rate of endocytosis between WT and Cav1-/- MEFs as shown by quantification of the mean fluorescence intensity of internalized Tfn or CTB. Error bars are ± SD (n= 30). Bars, (**A-B**) 10μm.

Figure S2. Anti-myc IgGs and Fab fragments do not affect the endocytosis mechanism of dysferlin in MEFs. WT Cav1 (not shown) and Cav1-/- MEFs were transfected with GFP-dysf. IgGs or Fab fragments of anti-myc antibodies were cointernalized with Tfn for 40min at 37^{o}C. There was no difference in the extent of internalization between anti-myc IgGs and Fab fragments in WT (not shown) and Cav1 -/- MEFs. Consistent with results shown in Figure 4, Cav1-/- MEFs internalize more IgGs or Fabs compared to WT Cav1 MEFs (not shown). Bars, 10μm.

Figure S1

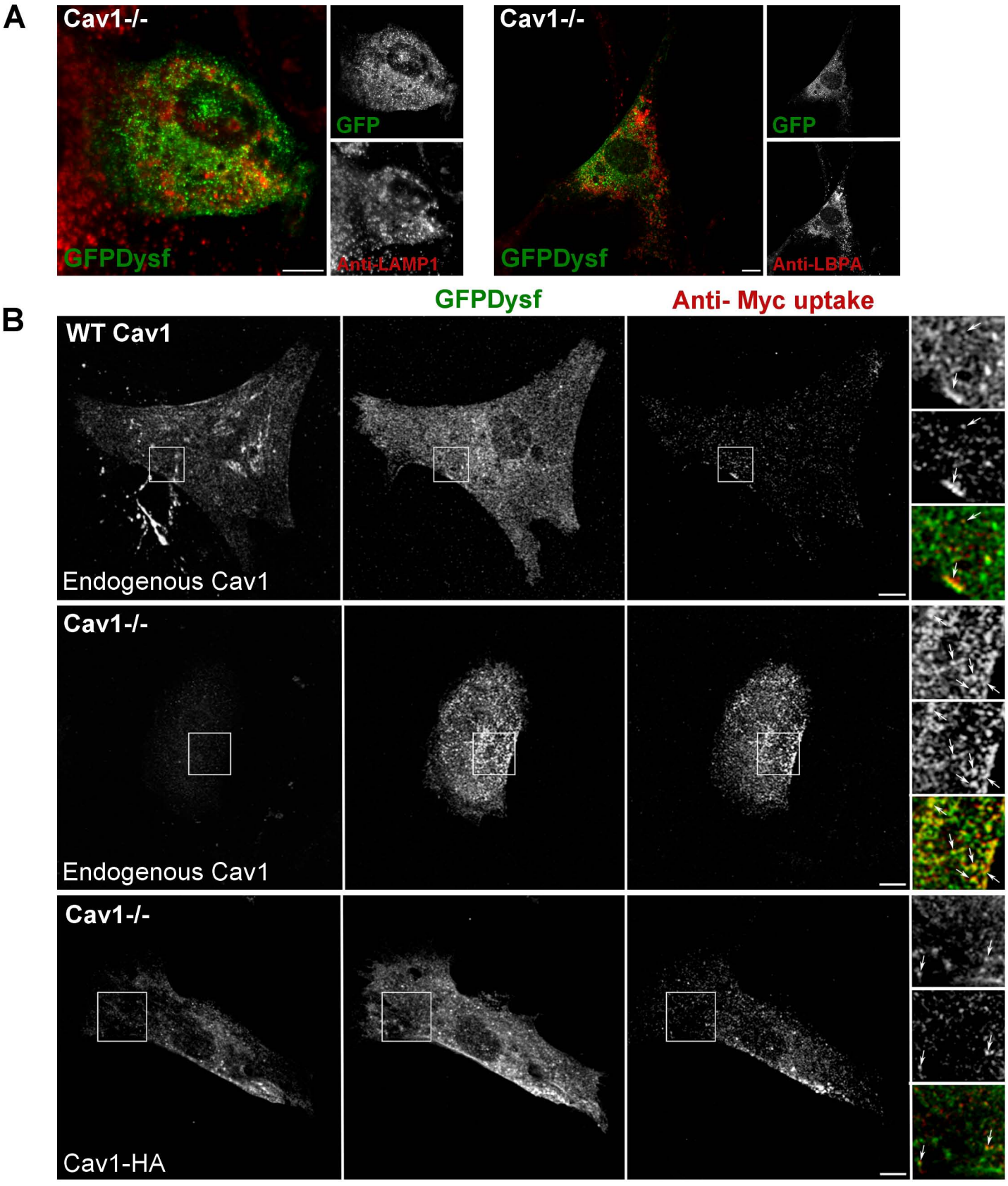
A
Cav1-/-
GFP
GFPDysf
Anti-LAMP1
Cav1-/-
GFP
GFPDysf
Anti-LBPA
B
GFPDysf
Anti- Myc uptake
WT Cav1
Endogenous Cav1
Cav1-/-
Endogenous Cav1
Cav1-/-
Cav1-HA
C
Average pixel intensity
100
80
60
40
20
0
WT Cav1 MEF
Cav1-/- MEF
10min Tfn uptake
10min CTB uptake

Figure S2

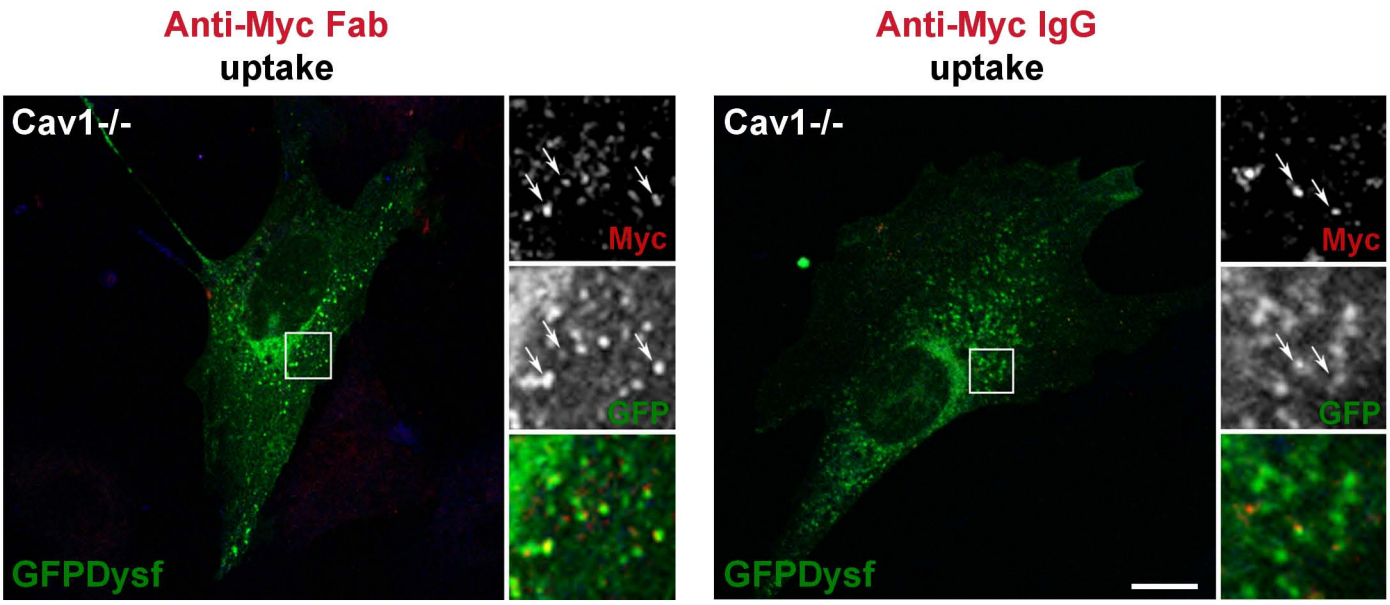
Anti-Myc Fab
uptake
Cav1-/-
Myc
GFP
GFPDysf
Anti-Myc IgG
uptake
Cav1-/-
Myc
GFP
GFPDysf

Caveolin Regulates Endocytosis of the Muscle Repair Protein, Dysferlin

Delia J. Hernández-Deviez, Mark T. Howes, Steven H. Laval, Kate Bushby, John F. Hancock and Robert G. Parton

J. Biol. Chem. 2008, 283:6476-6488.
doi: 10.1074/jbc.M708776200 originally published online December 20, 2007
